Tripyridinophane Platform Containing Three Acetate Pendant Arms: An Attractive Structural Entry for the Development of Neutral Eu(III) and Tb(III) Complexes in Aqueous Solution

Leygue, N.; Galaup, C.; Lopera, A.; Delgado-Pinar, E.; Williams, R.M.; Gornitzka, H.; Zwier, J.M.; García-España, E.; Lamarque, L.; Picard, C.

DOI
10.1021/acs.inorgchem.9b03345

Publication date
2020

Document Version
Final published version

Published in
Inorganic Chemistry

Inorganic Chemistry
Cite This: Inorg. Chem. 2020, 59, 1496−1512
Article
pubs.acs.org/IC

Tripyridinophane Platform Containing Three Acetate Pendant Arms: An Attractive Structural Entry for the Development of Neutral Eu(III) and Tb(III) Complexes in Aqueous Solution

Nadine Leygue,[†] Chantal Galaup,[†] Alberto Lopera,[‡] Estefanía Delgado-Pinar,[‡] René M. Williams,[§] Heinz Gornitzka,[∥] Jurriaan M. Zwier,[⊥] Enrique García-España,[‡] Laurent Lamarque,*[,⊥] and Claude Picard*[,†]

[†]Laboratoire de Synthèse et Physico-Chimie de Molécules d'Intérêt Biologique (SPCMIB), Université Paul Sabatier-Toulouse III/CNRS (UMR5068), 118 route de Narbonne, F-31062 Toulouse, France

[‡]Instituto de Ciencia Molecular (ICMOL), Universitat de València, C/Catedrático José Beltrán 2, 46980 Paterna, Spain

[§]Molecular Photonics Group, Van 't Hoff Institute for Molecular Sciences, University of Amsterdam, P.O. Box 94157, 1090 GD Amsterdam, The Netherlands

[∥]CNRS, LCC, Université de Toulouse, UPS, INPT, 205 Route de Narbonne, F-31077 Toulouse Cedex 4, France

[⊥]Cisbio bioassays, Parc Marcel Boiteux, BP 84175, 30200 Codolet, France

Supporting Information

ABSTRACT: We report a detailed characterization of Eu^{3+} and Tb^{3+} complexes derived from a tripyridinophane macrocycle bearing three acetate side arms (H_3tpptac). Tpptac^{3-} displays an overall basicity ($\sum \log K_i^H$) of 24.5, provides the formation of mononuclear ML species, and shows a good binding affinity for Ln^{3+} ($\log K_{LnL}$ = 17.5−18.7). These complexes are also thermodynamically stable at physiological pH (pEu = 18.6, pTb = 18.0). It should be noted that the pGd value of Gd-tpptac (18.4) is only slightly lower than that of commercially available MRI contrast agents such as Gd-dota (pGd = 19.2). Moreover, a very good selectivity for these ions over the endogenous cations ($\log K_{CuL}$ = 14.4, $\log K_{ZnL}$ = 12.9, and $\log K_{CaL}$ = 9.3) is observed. The X-ray structure of the terbium complex shows the metal coordinated by the nine N_6O_3 donor set of the ligand and one inner-sphere water molecule. DFT calculations result in two Eu-tpptac structures with similar bond energies (ΔE = 0.145 eV): one structure in which the water is coordinated to the metal ion and one structure in which the water molecule is farther away from the ion, bound to the ligand with an OH−π bond. By detailed luminescence experiments, we demonstrate that the europium complex in aqueous solution presents a hydration equilibrium between nine-coordinate, dehydrated [Eu-tpptac]^0 and ten-coordinate, monohydrated [Eu-tpptac(H_2O)]^0 species. A similar trend is observed for the terbium complex. Despite the presence of this hydration equilibrium, the H_3tpptac ligand sensitizes Eu^{3+} and Tb^{3+} luminescence efficiently in buffered water at physiological pH. Particularly, the terbium complex displays a long excited-state lifetime of 2.24 ms and an overall quantum yield of 33% with a brightness of 3600 M^{-1} cm^{-1}. Such features of Ln^{3+} complexes of H_3tpptac indicate that this platform appears to be particularly appealing for the further development of luminescent lanthanide labels.

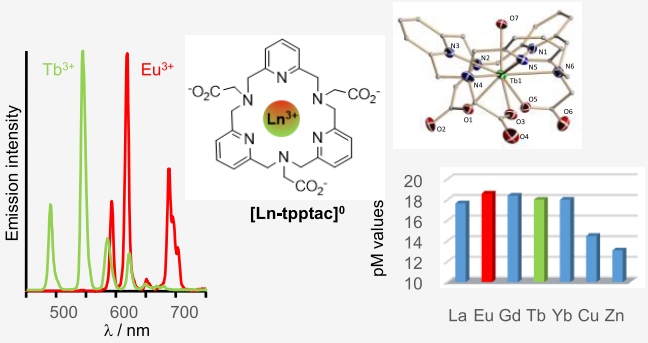

INTRODUCTION

In the last few decades, luminescent lanthanide complexes (especially those of Eu^{3+} and Tb^{3+}) have proven their worth as chemical tools for luminescent labels in bioanalytical and biomedical sciences. These lanthanide complexes have already found commercial use as probes in heterogeneous and homogeneous immunoassays for enzyme activity, binding assays, or applications in molecular biochemistry. These complexes have also been exploited for the specific detection of a variety of biorelevant parameters and analytes. Among them are pH value, temperature, reactive oxygen or nitrogen species (H_2O_2, $^{\bullet}OH$, $^1O_2$, and NO), metal cations (e.g., K^+, Cu^{2+}, and Zn^{2+}), anions (e.g., HCO_3^-, PO_4^{3-}, and F^-) and small organic molecules (e.g., uric acid, sugars, and thiols). Through fluorescence microscopy techniques, the benefit of lanthanide probes was also exploited for imaging cells, organisms, tissues, and laboratory animals. These numerous and various applications were summarized in several review articles that have appeared during the past five years.[1]

Received: November 14, 2019
Published: January 8, 2020

DOI: 10.1021/acs.inorgchem.9b03345
Inorg. Chem. 2020, 59, 1496−1512

These applications are due to the specific photophysical properties of luminescent Eu(III) and Tb(III) chelates. They display long emission lifetimes in the millisecond range, which allow the use of the time-resolved fluorescence technique, implementing simple and inexpensive instrumentation. In this technique, time-resolved measurements overcome the short-lived fluorescence background present in most biological materials and light scattering from the instrument optics, improving greatly the signal to noise ratio.[2] Their photophysical parameters (lifetime, shape of emission spectrum, intensity of the emission) are modulating depending on the environment of the lanthanide ion and thus allow the detection of analytes modifying this environment.[3] They are useful donors in Förster resonance energy-transfer assays to measure binding events, associated with the lengthening of the fluorescence lifetime of acceptors and measurable distances on the order of 100 Å.[4] Luminescent lanthanide chelates show also reduced photobleaching and higher photostability in comparison to organic fluorophores.[5] This feature is advantageous for imaging applications, allowing long and repeated exposures to excitation light, for instance, to study intracellular processes.

Among the numerous examples of luminescent lanthanide complexes, most of the investigated macrocyclic ligands are built on a limited number of coordinating core structures, such as cyclen (1,4,7,10-tetraazacyclododecane) or tacn (1,4,7-triazacyclononane) bearing side arms containing chromophoric unit(s) both to contribute to coordination and to act as an antenna, and acetic-, amide-, or phosphorus-based functional groups. Such ligands have been investigated because of the high thermodynamic stability of lanthanide complexes derived from dota (1,4,7,10-tetraazacyclododecane-1,4,7,10-tetraacetic acid) and nota (1,4,7-triazacyclononane-1,4,7-triacetate).[6] In order to extend the family of macrocyclic scaffolds suitable for luminescent lanthanide probes, we have been interested in designing lanthanide complexes based on a tpp platform for a long time (tpp, tripyridine pyridinophane = 2,11,20-triaza[3.3.3.](2,6)-pyridinophane, Chart 1). The tpp platform contains, in an 18-membered macrocyclic structure, 3 secondary amino groups and 3 pyridine rings which are known to generate the antenna effect.[7] The introduction of three monodentate side arms could fulfill the high coordination (8−10) required by Ln^{3+} ions in aqueous solutions for stable and soluble complexes in water. The presence of three pyridine units in the macrocyclic backbone might generate (i) a significant rigidification of the ligand bringing a positive effect on rapid complexation kinetics and high kinetic inertness in biological media of the resulting complexes, (ii) an antenna-to-metal photosensitization step occurring between partners in a rigid conformation, thus allowing improvement of the energy-transfer rates, (iii) an extension of conjugation of the pyridine ring through its 4-position to enhance the antenna effect, and (iv) enhancement of the absorption cross section of the ligand and consequently the brightness of the lanthanide complexes. The use of multiple antennae around a single lanthanide ion and the extension of conjugation of the pyridyl ring may be exemplified by the H_3tpatcn ligand (Chart 1) and related ligands.[8,9] Derivatives of H_3tpatcn are recently receiving particular attention for the design of very efficient luminescent lanthanide complexes emitting in the visible or near-infrared region and which benefit, in some cases, from nonlinear two-photon excitation.[9a,e]

Chart 1. Chemical Structures of H_3tpptac and Other Ligands Discussed in This Work

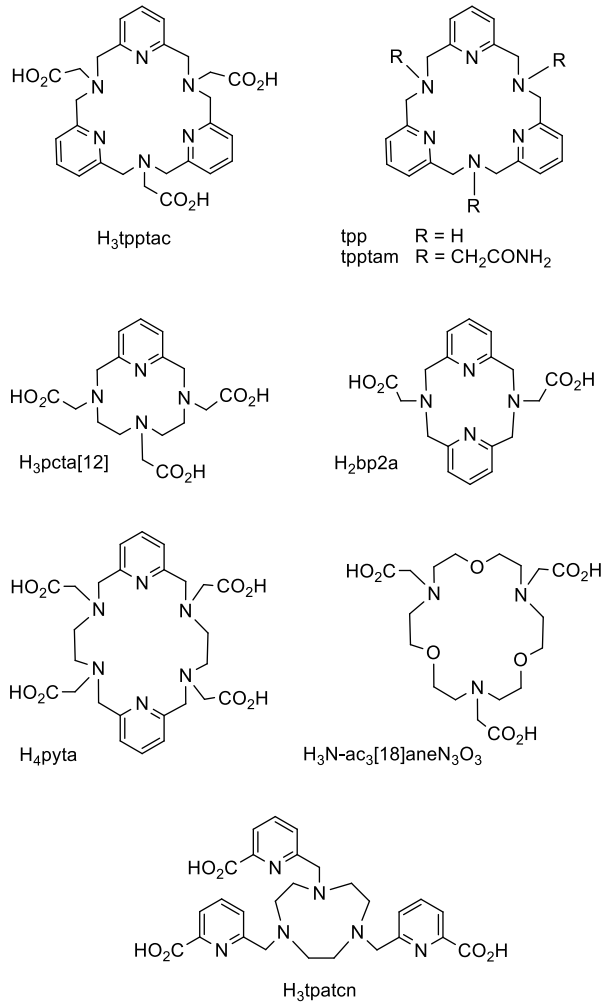

A few papers have been devoted to the tpp ligand and its derivatives. The first synthesis of tpp was reported by Lee et al. in 1996, but the binding properties of this ligand were only studied 17 years later.[10] In 2013, Castro et al. described the synthesis of its lanthanide complexes and their coordination properties in the solid state and in aqueous solution.[11] These authors also reported the same types of studies concerning Ln^{3+} complexes derived from a tpp platform containing three acetamide pendant arms (tpptam, Chart 1).[12] On the other hand, we reported recently a new synthetic strategy to access chelators derived from a tpp platform bearing acetate or mixed acetate/methyl phosphonate side arms.[13]

In this context, we were interested in evaluating the physicochemical properties of Ln^{3+} complexes derived from the H_3tpptac ligand (tripyridine pyridinophane triacetic acid, Chart 1), taken as a prototype of the tribranched tpp family. In this paper, we present a detailed investigation of the thermodynamic stabilities and photophysical properties of some Ln-tpptac complexes in aqueous solution. The thermodynamic properties of Ln(III) complexes (Ln = La, Eu, Gd, Tb, Yb) have been determined by using potentiometric titrations and compared to the stabilities of Cu^{2+}, Zn^{2+}, Mn^{2+}, and Ca^{2+} analogues. We also present a detailed photophysical study of the Eu^{3+} and Tb^{3+} complexes of this ligand to help in a better understanding of the role played by

DOI: 10.1021/acs.inorgchem.9b03345
Inorg. Chem. 2020, 59, 1496−1512

various factors that determine their luminescence properties. Moreover, the solid-state structure of the Tb complex is reported and the structure of the Eu complex is investigated by using density functional theory (DFT) calculations. Additionally, a comparison is made on the basis of structural, stability constant, and photophysical data for the complexes derived from H_3tpptac and H_3tpatcn ligands.

EXPERIMENTAL SECTION

Synthesis of Ln-tpptac Complexes. The synthesis of the ligand H_3tpptac was reported in a recent paper, and the ligand was isolated as its hexahydrochloride salt.[13] ^{1}H NMR (300 MHz, D_2O): δ 4.14 (s, 6 H, 3 × CH_2), 4.85 (s, 12 H, 6 × CH_2), 7.54 (d, J = 7.6 Hz, 6H, 6 × CH), 7.97 (t, J = 7.6 Hz, 3H, 3 × CH) ppm. Anal. Calcd for $C_{27}H_{30}N_6O_6$·6HCl·0.25H_2O: C, 42.79; H, 4.85; N, 11.09. Found: C, 42.81; H, 4.81; N, 10.94.

$LnCl_3$·6H_2O (55.7 μmol) in 2 mL of water was added to a solution of H_3tpptac·6HCl (40 mg, 50.6 μmol) in water (5 mL), with the pH adjusted to 6 with 0.1 N NaOH. The mixture was stirred for 24 h at room temperature, and then the pH of the solution was brought to 8 using a 1 N NaOH solution in water. After centrifugation, the solution was evaporated to dryness and the residue was purified by a Waters Sep-Pak column (C_{18}, 10 g), eluting first with pure H_2O to remove all inorganic salts and then with a H_2O/MeOH mixture to recover the complex. The Ln-tpptac complexes were isolated in 90−95% yields. An Arsenazo test confirmed the absence of free lanthanide ions, and the absence of free ligand was confirmed by mass spectrometry.

Eu-tpptac. MS (ESI)$^+$: m/z 683.1 (86%) [^{151}Eu-tpptac + H]$^+$, 685.1 (100%) [^{153}Eu-tpptac + H]$^+$, 705.1 (28%) [^{151}Eu-tpptac + Na]$^+$, 707.1 (31%) [^{153}Eu-tpptac + Na]$^+$, 721.1 (40%) [^{151}Eu-tpptac + K]$^+$, 723.1 (50%) [^{153}Eu-tpptac + K]$^+$. HRMS (ESI)$^+$: m/z calcd for [$C_{27}H_{27}N_6O_6{}^{151}$Eu + H]$^+$ 683.1269, found 683.1274; calcd for [$C_{27}H_{27}N_6O_6{}^{151}$Eu + Na]$^+$ 705.1088, found 705.1093. λ_{abs} (Tris buffer, pH 7.4): 267 nm (ε = 11900 M^{-1} cm^{-1}). λ_{em} (Tris buffer, pH 7.4, λ_{exc} = 267 nm) 578 (relative intensity, corrected spectrum 0.5), 593 (33), 618 (100), 650 (6), 689 nm (81).

Tb-tpptac. MS (ESI)$^+$: m/z 691.1 (100%) [Tb-tpptac + H]$^+$, 729.1 (20%) [Tb-tpptac + K]$^+$. HRMS (ESI)$^+$: m/z calcd for [$C_{27}H_{27}N_6O_6$Tb + H]$^+$ 691.1324, found 691.1346; calcd for [$C_{27}H_{27}N_6O_6$Tb + K]$^+$ 729.0883, found 729.0910. λ_{abs} (Tris buffer, pH 7.4): 267 nm (ε = 11000 M^{-1} cm^{-1}). λ_{em} (Tris buffer, pH 7.4, λ_{exc} = 267 nm) 490 (relative intensity, corrected spectrum 34), 544 (100), 585 (28), 622 nm (15).

Gd-tpptac. HRMS (ESI)$^+$: m/z calcd for [$C_{27}H_{27}N_6O_6$Gd + Na]$^+$ 712.1131, found 712.1163. λ_{abs} (Tris buffer, pH 7.4): 267 nm (ε = 11600 M^{-1} cm^{-1}).

Photophysical Experiments. Absorption measurements were done with a Hewlett-Packard 8453 temperature-controlled spectrometer in 10 mm quartz cuvettes. Emission and excitation spectra and luminescence decays at room temperature of the lanthanide complexes were measured using a Cary Eclipse spectrofluorimeter equipped with a xenon flash lamp source and a Hamamatsu R928 photomultiplier. At liquid nitrogen temperature, an LS-50B PerkinElmer spectrofluorimeter equipped with a xenon flash lamp source, a Hamamatsu R928 photomultiplier, and an L2250136 low-temperature accessory was used. Excitation spectra were corrected for the excitation light intensity, while emission spectra were corrected for the instrument response.

High-resolution spetra were recorded on a FluoTime 300 lifetime fluorescence spectrometer from PicoQuant (Berlin, Germany) using a Xe flash lamp (100 Hz repletion rate) for excitation at 267 ± 10.6 nm.

Lifetimes τ (uncertainty ≤5%) were determined by monitoring the decay at a wavelength corresponding to the maximum intensity of the emission spectrum, following pulsed excitation. They are the average values from at least five separate measurements covering two or more lifetimes. The luminescence decay curves were fitted by an equation of the form $I(t) = I(0)\exp(-t/\tau)$ by using a curve-fitting program.

The number of coordinated water molecules q was determined by comparison of the lifetimes of Ln(III) complexes in water (τ_H)/deuterated water (τ_D) and using eq 1[14]

$$q = A(1/\tau_H - 1/\tau_D) \quad (1)$$

where A = 1.05 for Eu(III) and 4.2 for Tb(III) and τ is given in ms, or the refined eq 2 taking into account the second coordination sphere interaction of water molecules[15,16]

$$q = A(1/\tau_H - 1/\tau_D - B) \quad (2)$$

where A = 1.11 and B = 0.31 for Eu(III), A = 5 and B = 0.06 for Tb(III), and τ is given in ms.

The luminescence quantum yields (uncertainty ±10%) were determined by the method described by Haas and Stein[17] using as standards [Ru(bpy)$_3$]$^{2+}$ in aerated water (Φ = 0.04)[18] for the Eu(III) complex or quinine sulfate in 1 N sulfuric acid (Φ = 0.546)[19] for the Tb(III) complex and corrected for the refractive index of the solvent. They were measured according to conventional procedures with diluted solutions (optical density <0.05).

The intrinsic luminescence efficiency (Φ_{Eu}) can be calculated by the equation below according to the literature[20]

$$\Phi_{Eu} = k_r/(k_r + \sum k_{nr}) = \tau_{obs}/\tau_R \quad (3)$$

where τ_{obs} is the emission lifetime determined experimentally and τ_R is the radiative lifetime, which was obtained from eq 4

$$1/\tau_R = k_r = A_{MD} \times n^3 \times (I_{\sum Fj}/I_{F1}) \quad (4)$$

where $I_{\sum Fj}$ is the integrated intensity of the entire emission spectrum, I_{F1} is the integrated intensity of the purely magnetic dipole transition $^5D_0 \rightarrow {}^7F_1$, A_{MD} is the emission probability of the magnetic dipole transition (14.65 s^{-1} for Eu(III)), and n is the refractive index of the solution (1.33 for aqueous solutions).

X-ray Crystallographic Study. All data were collected at low temperature using oil-coated shock-cooled crystals on a Bruker-AXS APEX II diffractometer with Mo Kα radiation (λ = 0.71073 Å). The structure was solved by direct methods,[21] and all non-hydrogen atoms were refined anisotropically using the least-squares method on F^2.[22]

CCDC-1964484 contains supplementary crystallographic data. These data can be obtained free of charge from The Cambridge Crystallographic Data Centre via www.ccdc.cam.ac.uk/data_request/cif.

Treatment of Disordered Water Molecules. All oxygen atom positions correspond to relatively high residual electron density. At the beginning of the water treatment each oxygen atom had an individual occupancy variable, and in order to avoid correlations between occupancies and U values, the U values of all water oxygen atoms have been refined with one common variable. The next step was to perform an accurate analysis of the occupancies of neighboring oxygen atoms, in order to avoid the presence of more than 100% of a water molecule in one single area, which would make no sense, from either a chemical or a crystallographic point of view. In order to stabilize the following anisotropic refinement, the occupancy values have been fixed based on the corresponding refined values. Altogether, 10.5 water molecules have been refined on 23 positions in order to absorb "diffuse water electron density".

Determination of Protonation and Stability Constants. The potentiometric titrations were carried out at 298.1 ± 0.1 K using 0.1 M KCl as the supporting electrolyte. The experimental procedure (buret, potentiometer, cell, stirrer, microcomputer, ...) has been fully described elsewhere.[23] The acquisition of the EMF data was performed with the computer program PASAT.[24] The reference electrode was an Ag/AgCl electrode in a saturated KCl solution. The glass electrode was calibrated as a hydrogen ion concentrated probe by the titration of previously standardized amounts of HCl with CO_2-free NaOH solutions and the equivalent point determined by Gran's method,[25] which gives the standard potential, $E°'$, and the ionic product of water (pK_w = 13.73(1)).

DOI: 10.1021/acs.inorgchem.9b03345
Inorg. Chem. 2020, 59, 1496−1512

Table 1. Properties of DFT Calculated Structures (in Vacuo) of the tpptac Complexes with Europium or Terbium[a]

compd	Ln−H_2O (Å)	Ln−O (Å)	Ln−O (Å)	Ln−O (Å)	μ (D)	E (eV)
Tb-H_2O (X)	2.385	2.341	2.365	2.366		
Tb-H_2O	2.686	2.214	2.233	2.236	14.42	−453.58088
Eu-H_2O (1)	2.926	2.302	2.318	2.325	14.30	−454.34394
Eu-H_2O (2)	5.401	2.286	2.281	2.280	15.87	−454.48902
Eu		2.281	2.281	2.281	15.21	−440.30423
Tb		2.227	2.227	2.227	15.04	−439.40109

[a]Given are selected distances between the lanthanide ion (Eu(III) or Tb(III)) and the oxygen atoms in the structure as well as the total dipole moment (μ) and the total bond energy (E, in eV). For comparison the distances for the X-ray structure are given as well (Tb−H_2O (X)).

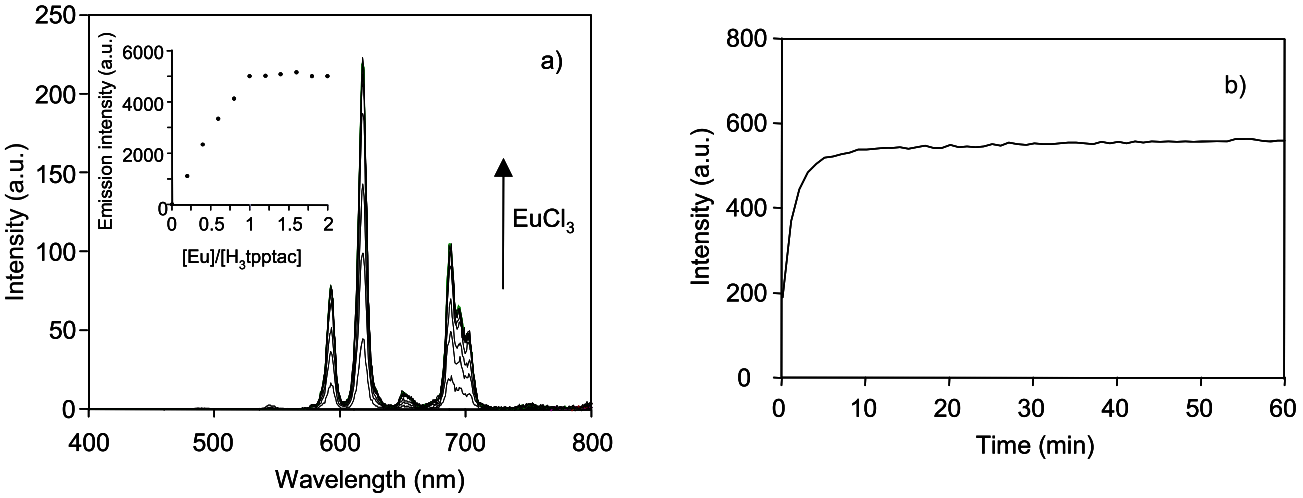

Figure 1. (a) Evolution of the emission spectrum of a solution of H_3tpptac upon the addition of increasing aliquots of $EuCl_3$ (0 → 2 equiv) in Tris buffer (pH 7.4). The inset shows the total emission intensity as the function of $EuCl_3$ added. (b) Plot of emission intensity of the $^5D_0 \rightarrow {}^7F_2$ transition (618 nm) vs time after mixing H_3tpptac and $EuCl_3$ (1 equiv) in Tris buffer (pH 7.4) at room temperature.

The computer program HYPERQUAD was used to calculate the protonation and stability constants.[26] The pH range investigated was 2.0−11.0, and the concentration of the ligand and metal ions was about 1×10^{-3} M with 1:1 M(III):L and M(II):L constant molar ratios. The different titration curves for each system (at least two) were treated either as a single set or as separated curves without significant variation in the values of the stability constants. Finally, the sets of data were merged together and treated simultaneously to give the final stability constants. The distribution diagrams were calculated using the HySS software.[27]

Spectra for pH-dependent UV−visible measurements ([H_3tpptac] = 5.0×10^{-5} M) were recorded with an Agilent 8453 UV−vis spectrometer at 293.15 K. Spectra for pH-dependent ^{1}H NMR measurements were recorded on a Bruker Advance DPX 300 MHz instrument operating at 299.95 MHz for ^{1}H. *tert*-Butyl alcohol was used as a reference standard (δ 1.24 ppm for ^{1}H).[28] Adjustments to the desired pH were made using drops of DCl and/or NaOD solutions. The pD was calculated from the measured pH values using the correlation, pH = pD − 0.4.[29]

Computational Methods. Structures were optimized with the ADF DFT package (SCM, version 2017) using the default SCF convergence criterion (1×10^{-6}) on the Lisa cluster of SURFsara.[30,31] As a starting structure, the X-ray structure of [Tb-tpptac(H_2O)]^0 was used, which was modified accordingly.

All geometry optimizations using unrestricted Hartree−Fock of the neutral complexes (with six unpaired electrons) were conducted using the zero-order regular approximation (ZORA) for relativistic effects[32] and Perdew and Wang (PW91) exchange and correlation for the GGA part of the density functional.[33] ADF basis sets TZ2P were used, with a small frozen core. A similar approach has been used for other metal complexes.[34] For the Eu-H_2O (1) complex (see Table 1), the starting structure was first minimized with a force field. ADF input and output files are provided as Supporting Information. The results were visualized with UCSF Chimera.[35]

RESULTS AND DISCUSSION

Synthesis and Characterization of Ln-tpptac Complexes. Luminescence spectroscopy was used to investigate the complex formation and stoichiometry of Ln-tpptac complexes in aqueous solution. Titration experiments for Tris buffer solution (pH 7.4) of ligand and $LnCl_3$ salts (Ln = Eu, Tb) showed that the addition of increasing amounts of ion up to 1 equiv resulted in an increase in the total integrated emission of the lanthanide, after which a plateau in the emission intensity was reached (Figure 1a). In these experiments, the metal luminescence lifetime is independent of the amount of Ln^{3+} salt added. These observations show that, at room temperature, the formation of the complex is fast and complete following the addition of 1 equiv of the lanthanide ion. The ESI$^+$-MS spectra, obtained with aqueous solutions containing the ligand and Eu^{3+} or Tb^{3+} in a 1:1 ratio are in agreement with results from luminescence titrations. These spectra are characterized by the absence of peaks ascribable to the free ligand and the presence of peaks corresponding to one positively charged species, [Ln-tpptac + H]$^+$ or sodium and potassium adducts. In addition, in order to obtain preliminary information about the rate of complex formation, the ligand ($c = 1.0 \times 10^{-6}$ M) was mixed with 1 equiv of Eu^{3+} in Tris buffer (pH 7.4) and the emission intensity of the metal was recorded with the passing of time (Figure 1b). This experiment showed that the ligand possesses rapid chelation kinetics under mild conditions (~10 min at

DOI: 10.1021/acs.inorgchem.9b03345
Inorg. Chem. 2020, 59, 1496−1512

room temperature). This fast formation kinetics can be attributed, at least in part, to preorganization of the H_3tpptac ligand due to the presence of three intracyclic pyridine rings. This observation is consistent with previous findings related to the faster formation rates of Ln-pcta complexes in comparison to those of Ln-dota complexes.[36] Consequently, the Ln^{3+} chelates derived from H_3tpptac were prepared at room temperature in aqueous solutions at pH 6 with an appropriate slight molar excess (ca. 10%) of the lanthanide salt to avoid the presence of free ligand and were isolated by purification using a Waters Sep-Pak column.

We have recorded the ^{1}H NMR of the Eu complex in D_2O at 298 K and pD 7.0 (Figure 2). This spectrum shows two sets

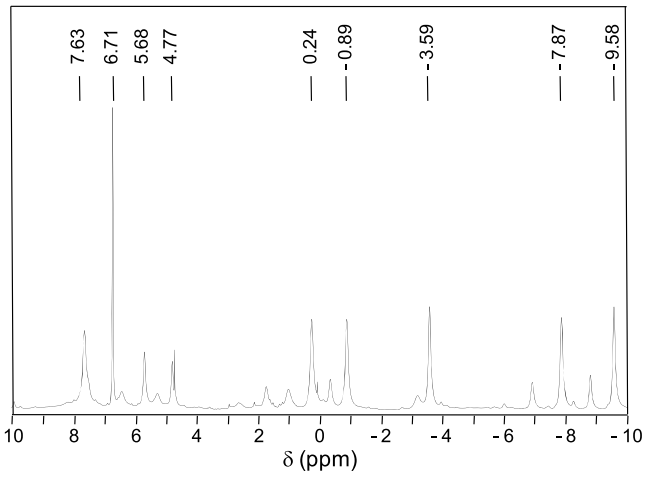

Figure 2. ^{1}H NMR spectrum of the Eu-tpptac complex recorded in D_2O solution at 298 K and pD 7.0 (500 MHz).

of signals spread between −10 and +10 ppm as a result of the paramagnetic lanthanide ion. The major set of nine signals may be related to a complex with an effective C_3 symmetry as reported by Castro et al. for Eu and Yb complexes derived from the tpptam ligand.[12] The second set of ^{1}H NMR signals is probably related to the presence of a second complex species in solution.

Despite several attempts, suitable crystals of the Eu complex for X-ray diffraction analysis could not be grown. On the other hand, single crystals of the Tb complex were obtained by slow evaporation of aqueous solution of the complex. A view of the structure of Tb-tpptac and selected bond lengths related to the coordination environment of the metal are given in Figure 3 (more complete information including crystal data and bond angles is given in Tables S1 and S2). The complex crystallizes as a mononuclear species in the triclinic space group $P\bar{1}$. The terbium ion is 10-coordinated, being bound to the six nitrogen atoms (three N_{tert} and three N_{py}) of the macrocyclic backbone and to the three oxygen atoms of the carboxylate functions, while a water molecule completes the metal coordination sphere. The shortest contacts are $Tb-O_{carboxylate}$ bonds with values between 2.34 and 2.37 Å, and even the $Tb-O_{water}$ distance (2.385 Å) is in the same range, while $Tb-N_{py}$ and $Tb-N_{tert}$ are significantly longer with average values of 2.67 and 2.71 Å, respectively. The metal cation and the ligand form a bowl-like structure with the carboxylate oxygen atoms as legs and the terbium and nitrogen atoms as the bowl hosting the water molecule coordinated to the metal center.

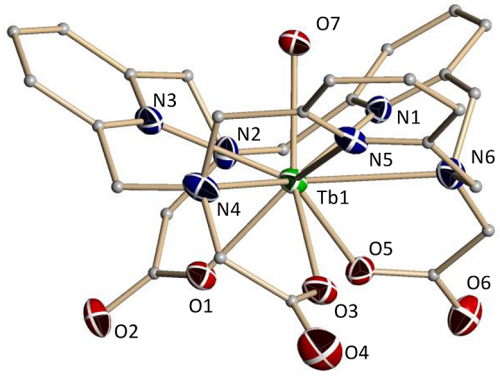

Figure 3. Structure of $[Tb\text{-tpptac}(H_2O)]^0$ in the solid state. Hydrogen atoms and noncoordinating water molecules are omitted, and carbon atoms are depicted as spheres for clarity. Tb, N, and O atoms are presented at the 30% thermal ellipsoid probability level. Bond distances of the metal coordination environment (Å): Tb−O1, 2.365(4); Tb−O3, 2.341(4); Tb−O5, 2.366(4), Tb−O7, 2.385(4); Tb−N1, 2.668(5), Tb−N2, 2.707(5), Tb−N3, 2.669(5); Tb−N4, 2.717(5); Tb−N5, 2.678(5); Tb−N6, 2.708(5).

Moreover, two complexes formed a head-to-head dimer in the unit cell (see Figure 4) with strong hydrogen bonds and an

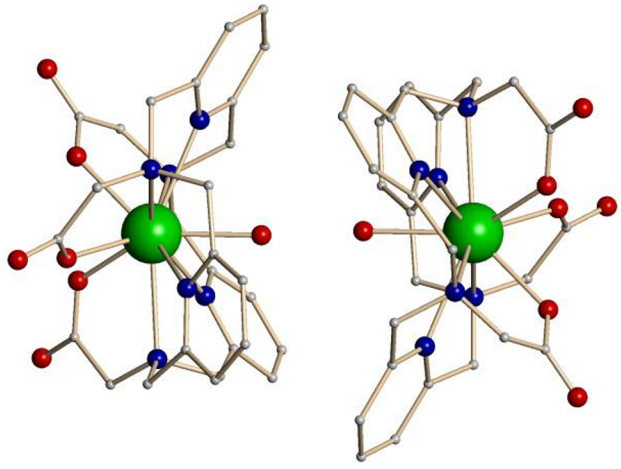

Figure 4. Dimeric structure of $[Tb\text{-tpptac}(H_2O)]^0$.

O−O distance of 2.214 Å. This dimer could be seen as a cagelike structure encapsulating the two water molecules. To the best of the authors' knowledge, such a dimer cage is unique in lanthanide structures. Furthermore, 10.5 molecules of water have been refined on a total of 23 positions, mainly located on the "back side" of the dimer, forming hydrogen bonds with the carboxylate oxygen atoms of the complexes with O−O distances varying from 2.66 to 3.01 Å.

A 10-coordinate environment of the Tb^{3+} ion is also observed in the solid-state structure of the analogue $[Tb\text{-tpptam}]^{3+}$, the tenth coordination site being occupied by an oxygen atom of a nitrate ion.[12] The average bond distances involving the donor atoms of the ligand (H_3tpptac or tpptam) are similar in the two corresponding terbium complexes. Particularly, no significant difference was observed in Tb−O (carboxylate or amide) bond lengths, although an amide oxygen has less negative charge density than a carboxylate oxygen. Additionally, we should note that the introduction of three acetate or acetamide side arms in the tpp platform

DOI: 10.1021/acs.inorgchem.9b03345
Inorg. Chem. 2020, 59, 1496−1512

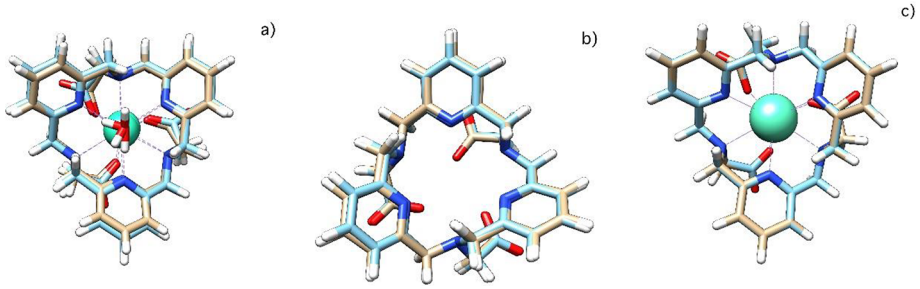

Figure 5. (a) Comparison of the structures of the two Tb(III) hydrate structures (X-ray Tb, brown; DFT Tb, blue). The RMSD for 70 atoms is 0.395 Å. (b) Comparison of the ligands of the calculated structures of the Tb(III) and Eu(III) hydrate structures (Tb, brown; Eu, blue; ions and water molecules removed before comparison). The RMSD for 66 atoms is 0.205 Å. (c) Comparison of the structures of the hydrate and non-hydrate Eu(III) structures (DFT) (Eu-tpptac, blue; Eu-tpptac-H_2O, in brown; water molecule removed before the comparison). The RMSD for 67 atoms is 0.013 Å.

lengthens the Tb−N_{py} and Tb−N_{tert} bond distances in the range 0.10−0.15 Å.[11] In [Tb-tpptac(H_2O)]^0, the Tb−$O_{carboxylate}$ distances are slightly shorter and the Tb−N distances are slightly longer than those reported for the 10-coordinate terbium complex derived from the related 18-membered dipyridinophane H_4pyta complex ([Tb-pyta]$^-$; average distances Tb−O 2.50 Å, Tb−N_{py} 2.58 Å, Tb−N_{tert} 2.63 Å).[37] On comparison of [Tb-tpptac(H_2O)]^0 and [Gd-N-ac$_3$[18]aneN_3O_3]^0 complexes, the average bond distances M−$O_{carboxylate}$ and M−N_{tert} are similar, whereas M−N_{py} distances are longer by 0.14 Å than those of M−O_{ether}, presumably because of a better flexibility of the H_3N-ac$_3$[18]aneN_3O_3 ligand.[38] Interestingly, [Gd-N-ac$_3$[18]aneN_3O_3]^0 is a 9-coordinated complex where the Gd^{3+} ion is surrounded by ligand donor groups with no coordinated inner-sphere water molecule. In [Tb-tpptac(H_2O)]^0, the coordinated water oxygen is 2.385 Å from the terbium cation, and this value is comparable with the Ln−OH_2 distance reported in the [Dy-tpptacm]$^{3+}$ complex and in other polyaminopolycarboxylate terbium complexes.[12,39]

Computational Results. DFT calculations were performed in order to get more structural and energetic information regarding five complexes. Results on the hydrated and nonhydrated Tb(III) and Eu(III) complexes with the tpptac ligand are presented in Table 1 and Figures 5−7. It is noted that our computational results contain two hydrated complexes of Eu with different water−ion distances. The structure of the tpptac ligand is very similar in all structures, but the positions of the metal ion and of the water molecule show (slight) differences.

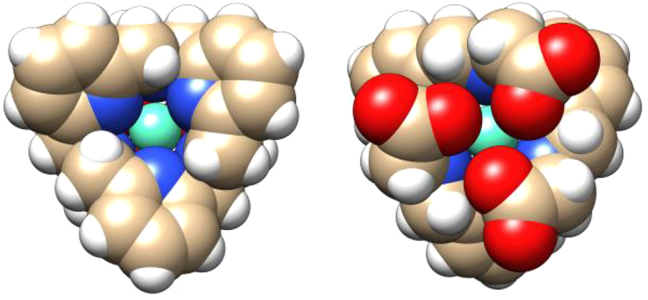

Figure 6. Space-filling representation of Eu-tpptac displaying the free water coordination site more clearly (left), as well as the triacetate side of the complex (right). DFT calculated structure.

The DFT calculations on [Tb-tpptac-H_2O]^0 reproduce the X-ray structure well (with a RMSD of 0.395 Å; RMSD = root-mean-square deviation of atomic positions), indicating the appropriateness of the method (see Figure 5a). Comparison of the calculated hydrated Eu and Tb complexes, however, results in nonoverlapping structures due to a different arrangement of the lanthanide ions in the cleft of the ligand. This is related to the metal ion−carboxylate distances (see Table 1). The ligand structures, however (removing ions and water), are very similar (RMSD of 0.205 Å; see Figure 5b). The calculated structures of the Eu complexes (with and without the water molecule) are virtually identical (RMSD for 67 atoms is 0.013 Å; see Figure 5c).

In the two hydrated complexes (of Eu(III) and Tb(III)), the distance between the water molecule and the ion and the carboxylate−ion distances are slightly different (see Table 1). On average the distance between the Tb(III) and the oxygen atom of the carboxylate group is 2.22 Å, while for the Eu(III) complex it is 2.31 Å. The europium ion is positioned slightly higher in the bowl of the ligand. (compare Tb-H_2O and Eu-H_2O (1) in Table 1). The large intrinsic dipole moment of the neutral metal complex, related to the metal ion−carboxylate interactions, is slightly modulated by the coordinating water molecule by its distance to the ion (from 15.2 to 14.3 D; see Table 1).

Figure 6 shows a space-filling representation of the Eu-tpptac structure clearly displaying the vacant water coordination site as well as the carboxylates protecting the lanthanide ion.

Slight modification of the starting structure for the DFT calculations of the Eu complex with a molecular mechanics force field (in comparison to starting from the structure based on the X-ray study of [Tb-tpptac(H_2O)]^0) results in two structures for the hydrate. These structures differentiate in the position of the water molecule. It is either coordinated to the Eu(III) ion or the water molecule interacts with the π systems of the ligand, showing a typical OH−π bond, with a distance of ∼2.6 Å between the proton and the center of the pyridine ring. The two binding modes of the water molecule to Eu-tpptac are presented in Figure 7 (data are given in Table 1). The calculated bond energies in vacuo indicate only a slight bond energy difference of 0.145 eV between these two structures. This energy difference is expected to be even smaller in an aqueous environment. The small energy difference between the metal-coordinated and noncoordinated water in the Eu complex agrees with the experimentally observed luminescent behavior (vide infra).

DOI: 10.1021/acs.inorgchem.9b03345
Inorg. Chem. 2020, 59, 1496−1512

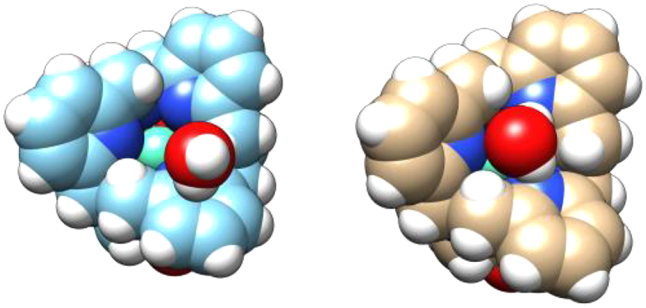

Figure 7. Space-filling representation of (right) [Eu-tpptac(H_2O)]^0 displaying the water coordination more clearly (Eu-H_2O (1)), as well as (left) a structure where the water molecule shows an interaction with the π system of the ligand (see Eu-H_2O (2) in Table 1 for numerical data). DFT calculated structures.

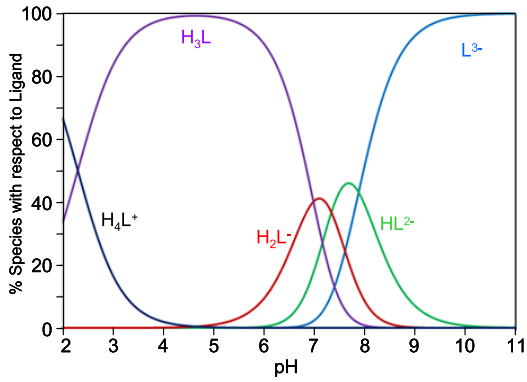

Figure 8. Distribution diagram for the ligand H_3tpptac as a function of the pH (H_3tpptac = H_3L, [H_3tpptac] = 10^{-3} M).

Protonation Constants of the Ligand and Stability of the Corresponding Complexes. The protonation constants of the ligand, defined in eq 5, were determined via potentiometric titrations in aqueous solution. The values are given in Table 2 along with previously reported values for macrocyclic polyaminopolycarboxylate ligands incorporating one or two pyridine ring(s), and H_4dota was used as the reference ligand. All of these data have been determined under the same experimental conditions: 0.1 M KCl ionic strength and 25 °C.

$$K_i^{H} = \frac{[H_iL]}{[H_{i-1}][H^+]} \quad (5)$$

The ligand tpptac^{3-} has nine basic centers, but only four constants could be determined in the pH range available for the potentiometric titrations. This is illustrated in the species distribution diagram of the ligand as a function of the pH (Figure 8). At physiological pH (7.4), the predominant species are the H_2L^- and HL^{2-} species and the full deprotonated species (L^{3-}) is the predominant species at pH >8.0. In comparison to the series of azapyridino macrocycles reported in Table 2, the protonation constants determined for tpptac^{3-} are rather low. The first protonation constant (log K_1^H = 7.89) is much lower (1.5−2.8 log units lower), and the first three protonation constants of this ligand range from ca. 8 to 7 logarithmic units with a separation of only 0.54 log unit (versus a 10.7−2.6 range with 0.5 < Δ log K^H < 3.6). The fourth constant determined for tpptac^{3-} (log K_4^H = 2.30) is similar to those of other ligands except for pyta^{4-}.

The first three protonation steps should occur on either the amine or pyridine groups, while the low value of the fourth step is typical of protonation of a carboxylate group linked to a protonated nitrogen atom. A survey of the literature data related to potentiometric studies of polyaminopolycarboxylate ligands with pyridine rings showed that the highest protonation constant corresponds to the protonation of a tertiary nitrogen atom, while the protonation of the pyridine is associated with log $K^H \approx 6$ or is not observed.[7a,42,46]

To get insight into this point, we have combined pH-dependent UV−visible spectroscopy and ^{1}H NMR measurements. The variations with pH of the absorbance of the pyridine band at 270 nm (Figures S5−S7) show a significant decrease in intensity (about 20%) from pH 9 to 5 in correspondence to the first three protonation steps, while they remain practically constant above and below this pH range. The variation of the ^{1}H NMR spectrum with pH is illustrated in Figure 9 and Figure S8. Due to the C_3 symmetry of the ligand, its ^{1}H NMR spectrum displays only two resonances for the pyridine protons and two singlets for the methylene spacers and the methylene groups of side arms. The ^{1}H signals attributable to the methylene protons of the acetate groups are those experiencing the largest upfield shifts ($\Delta\delta$ = 0.2 ppm) from pH 1 to 3, while the changes in the chemical shifts of the ^{1}H signals of the methylene groups of the macrocyclic core and of the aromatic signals are not significant in this pH range. At pH 6 the signals of the methylene groups of the macrocycle core are rather broad and undergo large upfield shifts ($\Delta\delta$ = 1.1 ppm) until the protonation is complete at pH 10. A similar trend is observed for the methylene groups of the acetate arms. Above pH 6 the aromatic signals also undergo upfield shifts ($\Delta\delta \approx$ 0.3−0.4 ppm).

In accord with the values derived for the protonation constants, above pH 9 the spectra remain practically unchanged, suggesting that there is no protonation process in highly basic medium. All these variations in the ^{1}H NMR spectra in combination with the changes in the UV−vis spectra suggest that the first three proton bindings of tpptac^{3-} would

Table 2. Logarithms of the Protonation Constants for tpptac^{3-} and Related Ligands in Aqueous Solutions at 25 °C and I = 0.10 M in KCl

	tpptac^{3-b}	pcta^{3-c}	bp2a^{2-e}	pyta^{4-f}	N-ac$_3$[18] aneN$_3$O$_3$$^{3-g}$	dota^{4-h}
log K_1^H	7.89(1)[a]	10.73(5), 10.6[d]	9.57(1)	9.37	9.57(2)	11.41
log K_2^H	7.35(1)	7.52(9), 7.6[d]	5.99(3)	8.81	8.15(3)	9.83
log K_3^H	6.99(1)	4.2(1), 4.4[d]	2.59(1)	5.80	7.67(1)	4.38
log K_4^H	2.30(1)	2.4(1)	2.22(1)	4.71	2.05(3)	4.63
$\sum$ log K_i^H	24.5	24.85	20.37	28.69	27.44	30.25

[a]Values in parentheses are standard deviations in the last significant figure. [b]This work. [c]Data from ref 40. [d]Data from ref 41. [e]Data from ref 42. [f]Data from ref 43. [g]Data from ref 44. [h]Data from ref 45.

DOI: 10.1021/acs.inorgchem.9b03345
Inorg. Chem. 2020, 59, 1496−1512

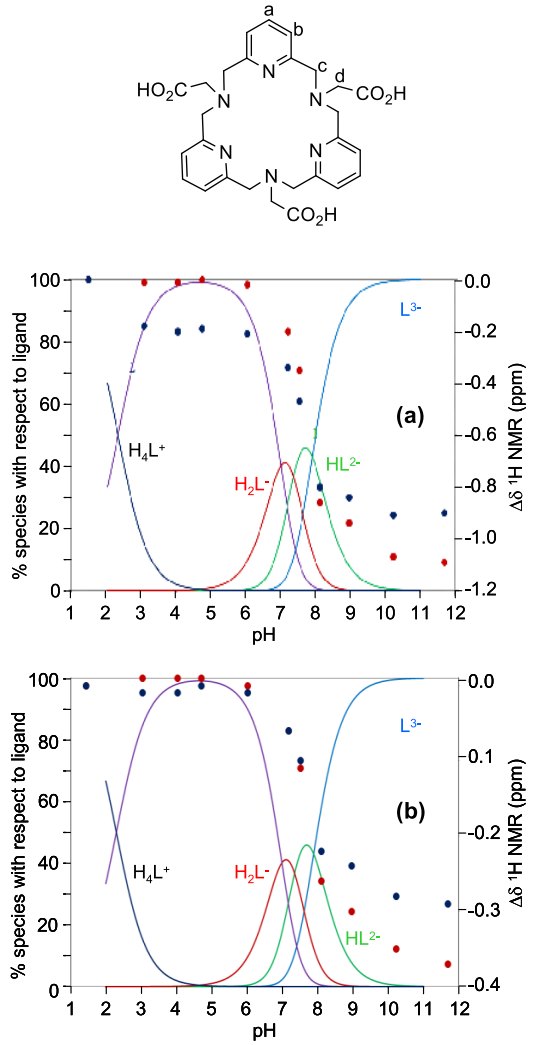

Figure 9. Plot of the species distribution diagram for H_3tpptac along with variations with pH of the ^{1}H NMR chemical shifts of (a) the methylene signals "c" (red circles) and "d" (blue circles) and (b) the aromatic signals "a" (red circles) and "b" (blue circles). $\Delta\delta$ was calculated in both drawings as the difference with respect to the δ values of the ligand at pH 1.45. pH values: 1.45, 3.05, 4.03, 4.71, 6.02, 7.19, 7.52, 8.11, 8.55, 8.96, 10.23, and 11.69. H_3tpptac = H_3L.

be somehow shared by the amine and the pyridine groups. The effective involvement of the pyridine rings in the protonation process may justify the low overall basicity of the ligand. Moreover, the basicity found for the first step of tpptac^{3-} is even lower than that reported for bp2a^{2-}, a related cyclic ligand having only two amino carboxylates and two pyridine rings. The crystal structure of this compound in its tetraprotonated form shows the location of the protons in the pyridine and carboxylate sites and not in the tertiary amine groups.[42]

The overall basicity ($\sum \log K_i^H$) of tpptac^{3-} (N_6O_3 donor set, 18-membered ring) is comparable to that of structurally related ligands such as pcta^{3-} and pc2a^{2-} (N_4O_3 and N_4O_2 sets, 12-membered ring).[40,42] The presence of three pyridine rings and the existence of only three aminoacetate groups contribute strongly to a lower overall basicity of tpptac^{3-} in comparison to that of pyta^{4-} (N_6O_4 donor set, 18-membered ring) with a decrease of about 4 log units. A significant change in the overall basicity is observed between the 18-membered macrocyclic ligands tpptac^{3-} and N-ac$_3$[18]aneN$_3$O$_3^{3-}$. The replacement of three dimethyleneoxy moieties by three pyridine rings leads to a decrease of 3 log units. A similar behavior is also observed for the 12-membered macrocycles pcta^{3-} and N-ac$_3$[12]aneN$_3$O^{3-}.[40,44] The value obtained for tpptac^{3-} is also clearly lower than that of dota^{4-}, anticipating a lower stability of the complexes reported here. Nevertheless, the low overall basicity of tpptac^{3-} is interesting from a coordination point of view, since it reduces the competition between the metal ions and the protons for the ligand which may lead to achieving high percentages of complexation even at low pH values (vide infra).

Complex stability constants, K_{ML}, have been determined for complexes formed with various Ln^{3+} ions (Ln = La, Eu, Gd, Tb, Yb) by potentiometric titrations and are reported in Table 3.

The complexation kinetics of H_3tpptac with these ions are fast enough for direct potentiometric titrations, avoiding the use of an out-of-cell (batch) method. The stability constants of the complexes have been calculated from the titration curves obtained at a 1:1 metal to ligand ratio; the best fitting was obtained by using the model that includes the formation of ML and MHL species in equilibrium. The speciation diagrams of Eu^{3+} and Tb^{3+} as representative examples are given in Figure 10 (other data are given in Figures S9−S11). These species distribution diagrams for the Ln complexes indicate that dissociation of the complexes takes place only at pH 3.8. At pH 3, the protonated complexes predominate, while the non-protonated complexes were the single species in aqueous solution at pH 5−11. The stability of the Ln-tpptac complexes is quite large and lies in the range of 17.5−18.7 log units, with the highest value observed for Eu-tpptac. The complex stability increases from the early lanthanides at about the middle of the series and slightly decreases for the heavier lanthanides. This tendency agrees with that reported for H_5dtpa and several macrocycles containing pyridine rings such as H_3pcta and H_2bpdpa.[36,47,48] This is in contrast with the macrocyclic polyaminocarboxylate ligands such as H_4dota, H_5pepa, and H_6heha, which form complexes of increasing stability all across the lanthanide series.[45,47]

As expected from the total basicity values, the present stability constants for Ln-tpptac complexes do not appear as large as the reported values for Ln-pyta (log $K_{LnL} \approx 22$) or Lndota (log K_{LnL} = 22−25).[43,45] In spite of the comparable total basicities of the ligands H_3tpptac and H_3pcta and the presence of two additional coordinating groups (two pyridine nitrogens) in the former, the stability of lanthanide complexes

Table 3. Logarithms of the Stability Constants of H_3tpptac with Different M^{3+} and M^{2+} Ions Determined in 0.1 M KCl at 25 °C

equilibrium reaction	La(III)	Eu(III)	Gd(III)	Tb(III)	Yb(III)	Cu(II)	Zn(II)	Mn(II)	Ca(II)
M + H + L ⇆ MHL[a]	20.86(3)[b]	21.74(6)	21.37(4)	21.23(4)	20.67(2)	20.83(2)	19.92(2)	18.98((2)	
M + L ⇆ ML	17.60(2)	18.69(4)	18.30(3)	17.96(3)	17.44(1)	14.39(5)	12.89(7)	12.97(4)	9.28(1)
pM (pH 7.4)	17.65	18.6	18.4	18.01	18.01	14.49	13.08		

[a]Charges omitted. [b]Values in parentheses are standard deviations in the last significant figure.

DOI: 10.1021/acs.inorgchem.9b03345
Inorg. Chem. 2020, 59, 1496−1512

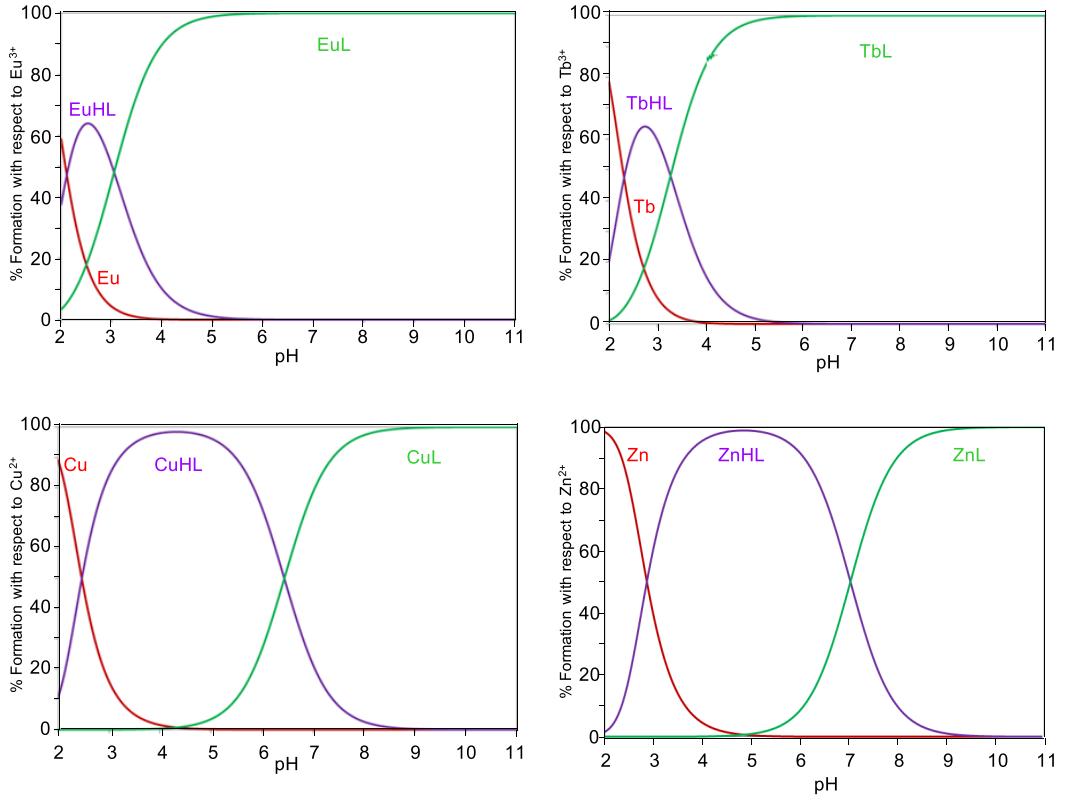

Figure 10. Distribution diagrams for the systems M^{3+}-H_3tpptac (M = Eu, Tb) and M^{2+}-H_3tpptac (M = Cu, Zn) as a function of pH (H_3tpptac = H_3L, [H_3tpptac] = 10^{-3} M).

Table 4. . pGd Values of Representative Chelators

	ligand							
	H_3tpptac	H_3pcta[a]	H_2bp2a[b]	H_4Pyta[c]	H_3N-ac$_3$[18]aneN$_3$O$_3$[d]	H_4dota[e]	H_5dtpa[f]	H_4edta[g]
pGd	18.4	17.3	13.3	19.25	15.7	19.2	18.9	15.3

[a]Calculated from data reported in ref 36; I = 1 M KCl. [b]Calculated from data reported in ref 42; I = 0.1 M KCl. [c]Calculated from data reported in ref 43; I = 0.1 M KCl. [d]Calculated from data reported in ref 44; I = 0.1 M KCl. . [e]Taken from ref 49; I = 0.1 M KCl.[f]Taken from ref 46a; I = 0.1 M KCl. [g]Calculated from data reported in ref 50; I = 0.1 M KCl.

is lower for H_3tpptac than H_3pcta (about 1.5 log units for the europium complex for example).[36] This may be related to the flexibility within these macrocycles, which outweighs basicity considerations. While H_3pcta has some flexibility region (diethylenetriamine core) as part of its macrocyclic ring, H_3tpptac does not have such flexibility. When a metallic complex is used under physiological conditions, its pM value is considered to be more accurate than its K_{ML} value. The pM value corresponds to the concentration of the free metal ion in the solution (pM = −log [M]) at pH 7.4) and is usually calculated in the presence of 100% ligand excess ($[ligand]_{total}$ = 10 μM, $[M]_{total}$ = 1 μM). These values are reported in Table 3. In order to compare the stability of Ln-tpptac to those of other lanthanide complexes, we have selected pGd values (Table 4) because of the greatest availability of stability constants for Gd^{3+} complexes. In addition, the relevance of these complexes as contrast agents in magnetic resonance imaging is well established. Table 4 shows that the H_3tpptac ligand has a pGd value higher than those presented by [Gd-edta]$^-$ and the related pyridine complexes [Gd-bp2a]$^+$ and [Gd-pcta]^0 and only slightly lower than those of commercially available MRI contrast agents such as [Gd-dtpa]$^{2-}$ and [Gd-dota]$^-$.

We have also investigated the complex stability of bioavailable cations, such as Cu^{2+}, Zn^{2+}, Mn^{2+}, and Ca^{2+}, in order to determine the selectivity of H_3tpptac. The corresponding speciation diagrams are reported in Figure 10 and Figures S12 and S13. Except for Ca^{2+}, the experimental data could be fitted with the introduction of a monoprotonated complex. In the case of the first three ions, the stability constants (K_{ML}) drop by 3−4.5 orders of magnitude in comparison to Ln stability constants. These results arise certainly from the more difficult adjustment of the ligand to these divalent metal ions, due to the inherent rigidity of the pyridine rings. With regard to Ln^{3+} ions, these M^{2+} ions have more stereochemical requirements for specific coordination chemistry. These log $K_{Cu,Zn}$ values are several orders of magnitude less than those of the related pyridine ligands H_3pcta and H_4pyta and reference polyaminocarboxylate ligands H_4dota and H_5dtpa (Table S3). As an example, the stability constants of [Cu-dota]$^{2-}$ and [Zn-dota]$^{2-}$ are about 7 and 10 log units higher, respectively. In comparison with these ligands, H_3tpptac forms Ln^{3+} complexes of very high selectivity over these bioavailable cations. We can also note that Ca^{2+} forms a complex of relatively low stability with H_3tpptac.

DOI: 10.1021/acs.inorgchem.9b03345
Inorg. Chem. 2020, 59, 1496−1512

Photophysical Properties of Eu-tpptac and Tb-tpptac Complexes. The main spectroscopic properties measured for Eu- and Tb-tpptac in air equilibrated Tris buffer solutions (50 mM, pH 7.4) are presented in Table 5. The photophysical properties obtained from the isolated complexes agree with those obtained when the complexes were formed in situ with equimolar solutions of $LnCl_3$ and ligand.

Table 5. Lifetimes, Overall Quantum Yields and the Number of Coordination Water Molecules of Ln-tpptac and Ln-tpatcn Complexes (Ln = Eu, Tb) in Tris Buffer (pH 7.4)

	Eu-tpptac	Tb-tpptac	Eu-tpatcn[a]	Tb-tpatcn[a]
λ_{max} (nm)	267	267	274	274
ε (M^{-1} cm^{-1})	11900	11000	14400	15800
τ_{H2O}^{298K} [τ_{H2O}^{77K}] (ms)	0.78 [0.82]	2.24	1.08	2.00
τ_{D2O}^{298K} [τ_{D2O}^{77K}] (ms)	1.99 [1.97]	3.34 [3.40]	1.47	2.14
$q(H_2O)$	0.82[b] [0.52][c]	0.62[b] [0.44][d]	−0.04	0.0
Φ_{ov}^{H2O} [Φ_{ov}^{D2O}] (%)	4.8 [11.8]	33 [50]	9.0	60.0

[a]Data from ref 8. [b]Number of coordination water molecules calculated according to the equations of Horrocks and Sudnick.[14] [c]Number of coordination water molecules calculated according to the equations of Supkowski and Horrocks.[15] [d]Number of coordination water molecules calculated according to the equations of Beeby et al.[16]

Europium Complex. The UV/vis absorption spectrum of the complex displays a broad emission band at 267 nm which can be attributed to $\pi-\pi^*$ transitions centered on the pyridyl moieties. In comparison to the free ligand, this absorption band is shifted toward lower energy, indicating an electronic interaction between the light-absorbing pyridine and the light-emitting europium center. The range of this red shift (~4 nm) is largely exemplified in the literature for the complexation of lanthanide ions by pyridine ligand.[7,51] The molar absorption coefficient (ε = 11900 M^{-1} cm^{-1}) is also in line with the presence of three pyridine units (ε_{py} = 3900 M^{-1} cm^{-1} for Eupcta).[52] Excitation (λ_{exc} = 267 nm) at 298 K gives a typical europium(III) emission spectrum containing the expected sequence of $^5D_0 \rightarrow {}^7F_J$ transitions with J = 0−4 being visible (Figure 11a). The strongest emission band is located at 618 nm, corresponding to the Eu(III)-centered $^5D_0 \rightarrow {}^7F_2$ hypersensitive transition (45% of the total integral intensity). The higher intensity of this transition in comparison to that of the magnetic-dipole-allowed $^5D_0 \rightarrow {}^7F_1$ transition points to a low symmetry of the ligand field around the metal. As expected, the metal luminescence excitation spectrum is located on the absorption range of the ligand and has shape similar to that of the absorption spectra, indicating a ligand-to-metal intersystem energy transfer (Figure 11b). No transition corresponding to the Eu(III) absorption levels, especially the $^7F_0 \rightarrow {}^5L_6$ transition (393 nm), is observable in the excitation spectrum.

At 298 K, the emission decay of Eu-tpptac can be fitted with a monoexponential function and is in the millisecond range (τ = 0.78 ms). This value is longer than that observed from the tpp ligand containing three acetamide pendant arms (τ = 0.57 ms) but shorter than reported for the H_3tptacn ligand functionalized with three picolinate arms (τ = 1.08 ms).[8,12] Experimental luminescence lifetimes of the Eu-tpptac complex were also recorded in D_2O solution, and lifetime data in H_2O and D_2O were analyzed in order to assess the hydration

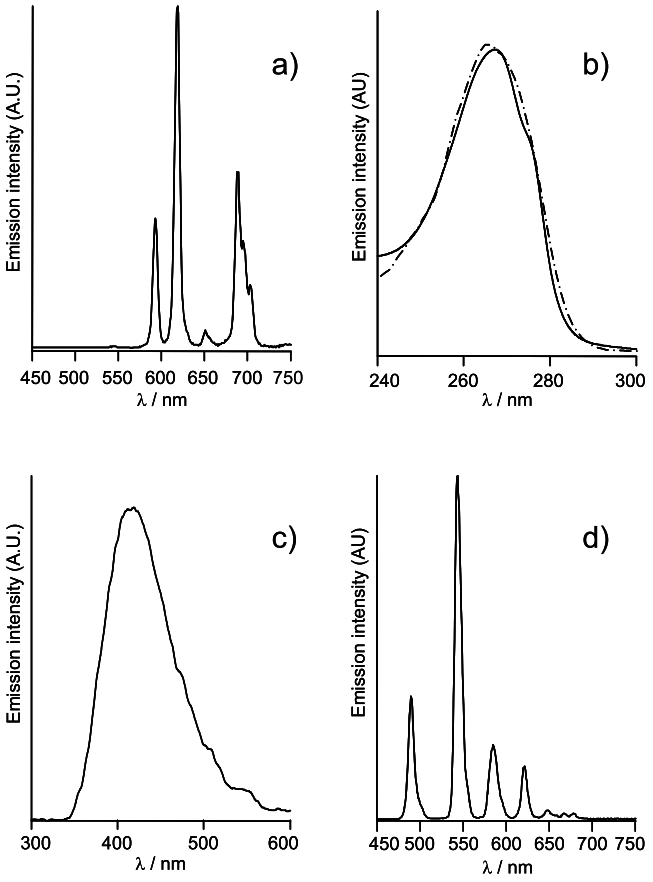

Figure 11. (a) Corrected emission spectrum of Eu-tpptac in Tris buffer (pH 7.4) at 298 K, λ_{exc} = 267 nm, and excitation and emission band passes 5 nm. (b) Normalized UV−vis (solid line) and corrected excitation (dashed line) spectra (λ_{em} = 618 nm) of Eu-tpptac in Tris buffer (pH 7.4). (c) Corrected emission spectrum of Gd-tpptac in MeOH/EtOH 4/1 solution at 77 K and λ_{exc} = 267 nm. (d) Corrected emission spectrum of Tb-tpptac in Tris buffer (pH 7.4) at 298 K, λ_{exc} = 267 nm, and excitation and emission band passes 5 nm.

number q of these complexes (i.e., the number of metal-bound water molecules). By using the phenomenological Horrocks and Sudnick equation,[14] the hydration state of the excited state of the complex is 0.82, which points to the presence of one inner-sphere water molecule in solution. We have also made use of a revised equation, established by Supkowski and Horrocks, taking into account interactions generated by water molecules in the second coordination sphere (i.e., closely diffusing water molecules).[15] By using this equation, a value of q = 0.52 was obtained. It should be noted that a similar q value (q = 0.5−0.6) was reported for the [Eu-tpptam]$^{3+}$ complex in aqueous solution by taking into account the influence of N−H oscillators on the luminescence lifetime.[12] This non-integer value may imply a hydration equilibrium between q = 0 and q = 1 species in solution.The presence of hydration equibria in solution involving 10-coordinate Eu(III) complexes has been recently reported.[53] In the case of an Eu(III) complex of a nonadentate ligand based on the pyclen macrocycle containing two picolinate and one acetate arms, Le Fur et al. reported the presence of a hydration equilibrium involving a monohydrated species (q = 1) with coordination number 10 and a 9-coordinate nonhydrated species (q = 0) species with an apparent hydration number of 0.4.[53] We have also used the affinity of the fluoride ion for the lanthanides to evidence the

DOI: 10.1021/acs.inorgchem.9b03345
Inorg. Chem. 2020, 59, 1496−1512

presence of directly coordinated water molecules.[54] As expected, the lifetime in H_2O was increased by a factor of 1.7 (τ = 1.33 ms) in the presence of saturating fluoride ion (0.4 M, KF). The incorporation of fluoride ion in the inner sphere of the metal was also reflected by important changes in the shapes of the $^5D_0 \rightarrow {}^7F_J$ transitions (J = 1, 2, and 4) and the I_{7F2}/I_{7F1} and I_{7F4}/I_{7F1} ratios (decrease of 15−20%, Figure S14). Similar luminescence lifetimes of Eu-tpptac were observed at 77 K, indicating that the hydration sphere of the metal does not change by lowering the temperature. This also suggests that a back-energy-transfer process between the acceptor manifold excited states of the europium ion (^5D_J, J = 0−3) and the donor triplet excited state $^3\pi\pi^*$ of the ligand or a quenching mechanism via low-lying LMCT (ligand-to-metal charge transfer) states does not occur for this complex. In either case of these quenching mechanisms, luminescence lifetimes would be significantly higher at 77 K than at 298 K.[55]

To gain additional information about the presence of an equilibrium of two species in aqueous solution, the emission spectrum was determined on a higher-resolution spectrum recorded at 298 K in H_2O (Figure 12). In the 583−600 nm region, the $^5D_0 \rightarrow {}^7F_1$ transition displays at least five components (lines and shoulders), suggesting the presence of more than one equivalent site for the Eu(III) ion.[56] The $^5D_0 \rightarrow {}^7F_0$ transition is broad (full width at half-height: 28 cm^{-1}), and asymmetric on its low-energy side, strongly indicative of the presence of two emissive Eu(III) species in solution. In fact, the $^5D_0 \rightarrow {}^7F_0$ transition occurs between nondegenerate energy levels; a single environment gives rise to only a single transition.[56] When this $^5D_0 \rightarrow {}^7F_0$ band was deconvoluted by using pure Lorentzian functions, a satisfactory fit of the data was obtained when two components were taken into account: a transition centered at 580.47 nm (47% of the emitted intensity) and a transition centered at 579.57 nm (53% of the emitted intensity). The presence of these two bands could be related to the existence of a hydration equilibrium. Indeed, two components of the $^5D_0 \rightarrow {}^7F_0$ transition separated by ∼0.5−1 nm were previously observed for differently hydrated species of Eu(III) complexes.[53,57] On the basis of these literature data, we tentatively assigned the component at high energy to the 10-coordinated species with q = 1 and the component at lower energy to the nonhydrated 9-coordinated species. The proportion of these two bands is in agreement with the apparent hydration number (0.52) obtained from luminescence lifetime measurements. Frey and Horrocks[58] showed that the energy of the $^5D_0 \rightarrow {}^7F_0$ transition ($\tilde{\nu}_{obs}$) can be calculated from eq 6

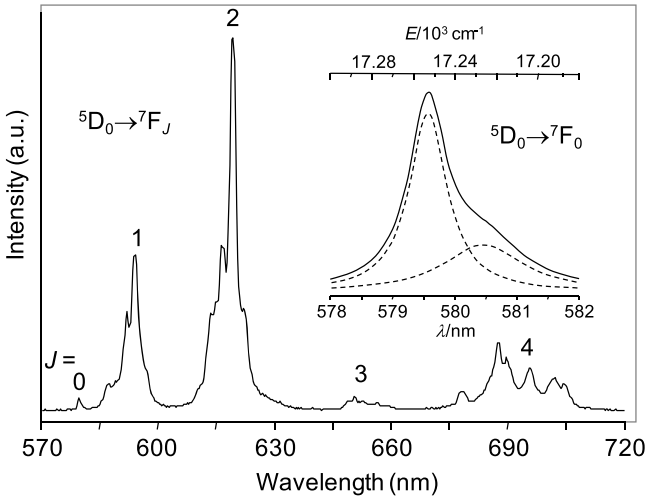

Figure 12. High-resolution emission spectrum of the Eu-tpptac complex in H_2O recorded at 298 K (λ_{exc} = 267 ± 10.8 nm). Insert: enlargement of the $^5D_0 \rightarrow {}^7F_0$ transition region and the corresponding individual Lorentzian signals.

$$\tilde{\nu}_{obs} = \tilde{\nu}_0 + C_{CN} \sum_i n_i \delta_i \quad (6)$$

where C_{CN} is a coefficient associated with the coordination number of the europium ion (1.0 for CN = 9 and 0.95 for CN = 10), n_i the number of coordinated atoms i, δ_i the energy shift parameter for atom i, and $\tilde{\nu}_0$ the energy of the $^5D_0 \rightarrow {}^7F_0$ transition of the free ion (17374 cm^{-1}). By using the nephelauxetic parameters δ_C = −15.53 cm^{-1} for the carboxylate oxygen, δ_N = −15.08 cm^{-1} for amine nitrogen, and δ_{Npy} = −16.67 cm^{-1} for the pyridine nitrogen donors,[59] the energy of the component at lower energy (17227 cm^{-1}) matches reasonably well with the theoretical value for a $N_3N^{py}{}_3O_3$ environment with no inner-sphere water molecule (17232 cm^{-1}). Considering a 9-coordinated complex where one amine nitrogen or pyridine nitrogen donor is substituted by a water molecule ($N_2N^{py}{}_3O_3O_w$ or $N_3N^{py}{}_2O_3O_w$ environment), the application of eq 6, with δ_w = −10.34 cm^{-1} for inner-sphere water molecule,[59b] gives theoretical estimations of $\tilde{\nu}$ in worse correlation ($\Delta\tilde{\nu}$ > 10 cm^{-1}). This is in agreement with an NMR study and computational work where no indication is found for a sp^3 nitrogen atom inversion. When the C_{CN} value of 0.95 for a total coordination number of 10 ($N_3N^{py}{}_3O_3O_w$ environment) is taken into account, the phenomenological equation predicts a transition energy of 17230 cm^{-1} for the species observed at 17254 cm^{-1}. This inconsistency can be tentatively explained by diminishing the nephelauxetic parameters of coordinating atoms in a 10-coordination environment but arises certainly from the very poor number of decadentate species used for the determination of the C_{CN} value (CN = 10), in contrast with the determination of the C_{CN} value for nonadentate species.[58] For Eu-tpptac, a better fit between experimental and calculated values implies a C_{CN} value of 0.8 for decadentate species ($\tilde{\nu}_{calc}$ = 17252 cm^{-1}). For similar reasons, Latva and Kankare proposed a C_{CN} value of 1.21 for a total coordination number of 8 instead of the original value of 1.06 proposed by Frey and Horrocks.[58,59b]

The overall quantum yields were determined in 50 mM Tris-buffered solutions at pH 7.4 in H_2O (Φ_{H2O} = 4.8%) and in D_2O (Φ_{D2O} = 11.8%), using $[Ru(bpy)_3]Cl_2$ as a reference. These values take into account the efficiency of the overall energy-transfer process from the pyridyl sensitizers to the europium ion states. The overall quantum yield of sensitized emission (Φ_{ov}, as determined experimentally) can be broken up into three contributions (eq 7)[60]

$$\Phi_{ov} = \eta_{isc} \times \eta_{Et} \times \Phi_{Ln} = \eta_{sens} \times \Phi_{Ln} \quad (7)$$

where η_{isc} and η_{Et} reflect the efficiency of intersystem crossing ($^1\pi\pi^* \rightarrow {}^3\pi\pi^*$) and ligand to metal energy transfer ($^3\pi\pi^* \rightarrow$ Ln*), respectively. These two terms correspond to the sensitization efficiency, η_{sens} ($\eta_{sens} = \eta_{isc} \times \eta_{Et}$). The intrinsic quantum yield, Φ_{Ln}, corresponds to the quantum yield of the lanthanide ion when it is excited into its own levels. In the case of the europium(III) ion, Φ_{Eu} may be calculated from the

DOI: 10.1021/acs.inorgchem.9b03345
Inorg. Chem. 2020, 59, 1496−1512

experimental data (spectrum, Φ_{ov}, and lifetimes) according to eqs 3 and 4 in the Experimental Section. These calculated photophysical parameters for Eu-tpptac are gathered in Table 6. In H_2O solution, we calculated Φ_{Eu} = 18%, corresponding to

Table 6. Calculated Photophysical Parameters for Eu-tpptac and Eu-tpatcn Complexes in Tris Buffer (pH 7.4) and Energy Information of Triplet State

	Eu-tpptac in H_2O	Eu-tpptac in D_2O	Eu-tpatcn in H_2O[a]
$I_{\sum Fj}/I_{F1}$[b]	6.7	6.6	8.3
k_r (s^{-1})[c]	230	228	295
k_{obs} (s^{-1})[b]	1282	502	926
Φ_{Eu} (%)[c]	18	45	32
η_{sens} (%)[c]	27.0	26.7	28.2
Φ_{ov} (%)[b]	4.8	11.8	9.0
Σk_{nr} (s^{-1})[c]	1048	279	627
$E(^3\pi\pi^*)$ (cm^{-1})[d]	23900	23900	24000

[a]Data from ref 8. [b]Experimentally measured parameters. [c]Calculated parameters; see the Experimental Section. [d]Determined as the λ_{max} value of the phosphorescence spectra of the corresponding Gd(III) complexes.

a poor metal-centered emission. This parameter is mainly dependent on the presence of metal-coordinated water molecules, and consequently we calculate Φ_{Eu} = 45% in D_2O, in agreement with a rather efficient metal-centered emission and a satisfying structural and electronic optimization of the metallic coordination sphere. As expected, the sensitization efficiencies, which are independent of the presence of inner-sphere water molecules, are comparable in H_2O and D_2O solutions. The calculated value of η_{sens} (27%) is modest, although the antennae are ligated to the metal. The sensitization efficiency is highly dependent on the energy gap between the sensitizer excited state ($^3\pi\pi^*$) and the Ln(III) emitting level. The triplet state energy of the ligand under the perturbation caused by coordination to a lanthanide ion was measured as usual from the ligand phosphorescence spectrum of the corresponding gadolinium complex. At 77 K in a 4/1 methanol/ethanol mixture, Gd-tpptac exhibits ligand phosphorescence as a broad emission band between 350 and 550 nm with a maximum at around 418 nm and an emission lifetime of 17.2 ms (Figure 11c). Unfortunately, due to the lack of vibrationally structured phosphorescence emission bands, it is not possible to determine the $\tilde{\nu}_{00}$ value of the triplet level in the complex. However, we can regard that this triplet energy level lies in the 28600−23900 cm^{-1} range (i.e., the domain ranging from the left edge to the maximum of the phosphorescence spectra). Looking at this energy range, we think it is likely that the excitation energy may be primarily transferred to the $^5D_3$ (24500 cm^{-1}), $^5D_2$ (21500 cm^{-1}), or $^5D_1$ (19000 cm^{-1}) levels of the Eu(III) ion that decay nonradiatively to the lower-lying $^5D_0$ (17300 cm^{-1}). During this transfer from upper ^5D_J levels to the emitting $^5D_0$ level, quite significant energy losses can consequently take place, diminishing the overall quantum yield.

At last, we explored the resistance of Eu-tpptac in regard to metal dissociation and this behavior was monitored by luminescence experiments. We challenged the complex at room temperature with 150 equiv of competing H_5dtpa ligand in Tris buffer at pH 7.4 (K(Eu-dtpa) = 2.5 × 10^{22}). Under these conditions, the shape of the emission spectrum, the total intensity, and the lifetime of Eu-tpptac did not differ after 48 h incubation. This result suggests a high kinetic inertness of the complex. Similar results were observed when Eu-tpptac (10 μM) was challenged by an excess of Cu^{2+} and Zn^{2+} cations (1 mM). These results indicate the high resistance of the complex to transchelation and transmetalation reactions.

Terbium Complex. Under excitation into the ligand absorption, the emission spectrum of Tb-tpptac displays four distinct peaks at 490, 544, 585, and 622 nm with weak signals in the 640−700 nm range which are assigned to the $^5D_4 \rightarrow {}^7F_J$ transitions (J = 6−0) of the Tb^{3+} ion (Figure 11d). The spectrum is dominated by the $^5D_4 \rightarrow {}^7F_5$ transition at 544 nm, which gives an intense green luminescence output for the solution. In contrast to the Eu^{3+} ion, the large degeneracy of excited and ground states of the Tb^{3+} ion does not enable a detailed analysis of the composition of the inner coordination sphere of the complex. The lifetime determined in Tris-buffered solution is 2.24 ms at room temperature, among the highest values of Tb^{3+} complexes based on pyridinic chromophores in aqueous solution.[7b,51c,52,61] The experimentally determined numbers of coordinating water molecules are q = 0.62 and q = 0.44 by using the original equation and the revised equation taking into account the outer-sphere contribution, respectively.[14,16] This result points to the presence of a hydration equilibrium as for the europium complex. Lifetimes of the $^5D_4$ level in D_2O solution at 298 and 77 K are similar, indicating that a back energy transfer $^5D_4$ (Tb) → $^3\pi\pi^*$ (ligand) is not operative. According to the work of Latva et al., the energy gap $^5D_4$−$^3\pi\pi^*$ ($\Delta E \geq$ 3400 cm^{-1}) is so large as to prevent back energy transfer.[62] The overall luminescence quantum yield of the complex is 7-fold higher than the corresponding Eu(III) yield, reaching the substantial value of 33% in aqueous solution. This can be attributed to the lower susceptibility of Tb^{3+} vs Eu^{3+} luminescence toward quenching by the hydroxyl groups of the solvent, and especially to the lower gap of the triplet state of the H_3tpptac ligand with the terbium emitting state. The value of Φ_{ov} in D_2O (50%) is in accordance with the dependence of the luminescence quantum yields of Tb(III) polyaminocarboxylate chelates on the triplet state energies of the ligand.[62] In addition, we can note that Tb-tpptac displays a quantum yield (33%) and a brightness (B = 3600 M^{-1} cm^{-1}) close to those reported for a terbium-based commercial luminescent probe (Φ_{ov} = 32% and B = 3600 M^{-1} cm^{-1}) for Tb-(DTPA-Cs124).[63]

Comparison between Ln-tpptac and Ln-tpatcn Complexes. It is interesting to compare the thermodynamic stability and the photophysical performances of Ln-tpptac complexes to the corresponding complexes formed with the H_3tpatcn ligand reported by Mazzanti and co-workers.[8] This ligand (Chart 1) can be considered as the prototype of ligands which have been designed to sensitize several lanthanide ions (Eu^{3+}, Tb^{3+}, Sm^{3+}, Yb^{3+}) and to maximize the excitation wavelength and the brightness of the corresponding complexes.[9] The two ligands share structural features such as a macrocyclic backbone, a similar ligand denticity (nonadentate ligand), a similar number and type of coordinating atoms, and an overall neutral charge of their Ln(III) complexes. However, they differ from one another in the size of the macrocyclic backbone (18-membered vs 12-membered) and in the arrangement of pyridine chromophoric units (intracyclic vs pendant arms).

Despite the great attention paid recently to the study of the ligand H_3tpatcn and derivatives for the development of

DOI: 10.1021/acs.inorgchem.9b03345
Inorg. Chem. 2020, 59, 1496−1512

luminescent lanthanide probes, only two thermodynamic studies of their metallic complexes have been undertaken. The stability constant for Ln-tpatcn was determined only for the terbium complex and was reported as K_{TbL} = 17.4 (pTb = 14.9) by Mazzanti and co-workers.[8] More recently, Tripier and co-workers reported stability constants for Cu-tpatcn (log K_{CuL} = 16.21) and Zn-tpatcn (log K_{ZnL} = 15.95) in a work on copper-based radiopharmaceuticals.[64] Although the basicity of tpatcn^{3-} ($\sum$ log K_i^H = 25.8) is higher than that of tpptac^{3-} ($\sum$ log K_i^H = 24.5), the stability constant of Tb-tpatcn is 0.6 log unit lower than our calculated log K_{ML} value of 18.0 for Tb-tpptac. This suggests a geometrically more favorable conformation of the latter ligand for the coordination of Tb^{3+} in comparison to that of the former. Additionally, our ligand can be also regarded for the terbium complex as a better ligand than H_3tpatcn over the pH range 5−10, as illustrated in Figure 13. Moreover, the enhanced stability of Tb-tpptac and

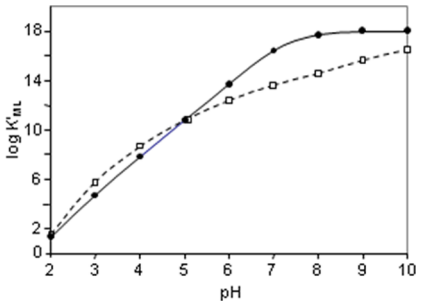

Figure 13. Variation of the conditional stability constant of the Tb^{3+} complexes of H_3tpptac (●) and H_3tpatcn (□) as a function of the pH.

mainly the reduced stability of Cu-tpptac or Zn-tpptac significantly improved the selectivity constant of this ligand, log K(Tb/Cu) = 3.6 and log K(Tb/Zn) = 5.1, over that of H_3tpatcn, log K(Tb/Cu) = 1.2 and log K(Tb/Zn) = 1.5. Overall, our ligand can be regarded as a better and more selective chelator for Ln^{3+} in comparison to H_3tpatcn from a thermodynamic point of view.

In contrast with Eu- and Tb-tpptac, luminescence experiments showed than Eu- and Tb-tpatcn exist as single and nonhydrated species in aqueous solution. This was further demonstrated by an X-ray structure of Tb-tpatcn in which the 9-coordinated Tb^{3+} ion is only bound by the 9 donor atoms of the ligand, with no water molecule present in its coordination sphere. An inspection of the photophysical data of Eu-tpptac and Tb-tpatcn complexes (Tables 5 and 6) deserves several comments. (i) In comparison to Eu-tpptac, Eu-tpatcn displays an absorption maximum shifted by 7 nm and a ε value 1.2 higher, due to the connection of a carboxylate substituent at the 2-position of the pyridine ring. (ii) The efficiency of energy transfer, η_{sens}, is similar for the two kinds of complexes in the range 25−30%. Looking at the triplet state energies, the position is fairly similar (23900/24000 cm^{-1} considering the maximum of the emission band in corresponding Gd^{3+} complexes), so that the energy gap ($^3\pi\pi^* \rightarrow$ Eu*) should be comparable for both ligands. (iii) In the two complexes, the main factor that limits the observed overall quantum yield is the rather low efficiency of energy transfer, η_{sens}. (iv) Due to the presence of a hydration equilibrium, the emission lifetime of Eu-tpatcn is longer and the overall quantum yield higher in H_2O solution than those observed for Eu-tpptac. On the other hand, we can note that Eu-tpptac shows in D_2O higher values for these two luminescence parameters in comparison to Eu-tpatcn in H_2O. In the same way, Tb-tpptac displays in D_2O a higher emission lifetime than Tb-tpatcn and an emission quantum yield in the same range.

CONCLUSIONS

Some lanthanide complexes derived from a tpp platform and various side arms have been recently reported, but their thermodynamic stability constants and detailed photophysical properties were not undertaken. In this work, we have studied these physicochemical properties of lanthanide complexes derived from the H_3tpptac ligand, taken as a prototype of the tribranched tpp family.

The stability constants of Ln-tpptac complexes were determined by pH-potentiometry and are in the range 3.0 × 10^{17} to 5.0 × 10^{18}. Importantly, these Ln^{3+} complexes are thermodynamically stable at physiological pH with pLn values in the range of those of Ln-dota and Ln-dtpa complexes. The H_3tpptac ligand shows also a great selectivity for lanthanide ions versus biogenic metal ions (Cu^{2+}, Zn^{2+}, Mn^{2+}, and Ca^{2+}), preventing transmetalation reactions.

Analysis of emission spectrum and emission lifetimes of the Eu^{3+} complex shows that this complex exists in aqueous solution as a mixture of non-hydrated and monohydrated species. From luminescence lifetime data, a similar behavior is assumed for the Tb^{3+} complex. DFT results show a small energy difference between water coordinated to the Eu(III) ion within the bowl of the ligand and water that interacts with the π system of [Eu-tpptac]^0, which agrees with the experimentally observed luminescent properties. A molecular structure determination of the Tb^{3+} complex by X-ray crystallography is fully consistent with the presence of a 10-coordinated species, implying all coordinating atoms of the ligand and one inner-sphere water molecule. Owing to the high value of ligand triplet state energy and the greater sensitivity of Eu^{3+} vs Tb^{3+} luminescence toward quenching by metal-coordinated water molecules, H_3tpptac is a better sensitizer of Tb^{3+} than of Eu^{3+} ion. Despite the presence of a hydration equilibrium, the terbium complex displays a long excited state lifetime of 2.4 ms and a high overall quantum yield of 33% in H_2O solution at pH 7.4. On the other hand, the europium complex displays significant luminescence parameters in D_2O solution (τ = 1.99 ms and Φ_{ov} = 11.8%).

On the basis of these data, the H_3tpptac ligand seems to be an attractive structural entry for constructing efficient Ln^{3+}-based luminescent probes in aqueous solution. Further refinement of the ligand structure may arise from the following. (i) The absorption maximum should shift to a longer wavelength more suitable for biological applications and a higher extinction coefficient to increase the brightness of complexes. In this direction, the introduction of a suitable substitution into the pyridine units is well documented.[9h] (ii) The capacity of a water molecule to bind the metal ion should be eliminated by, for example, the substitution of carboxylate groups by phosphate or phosphinate groups.[13,65] (iii) The ligand should be able to conjugate the complexes to biomolecules (antibody, protein, ...). The synthetic pathway of a tpp platform allows the introduction of a reactive group on a single pyridine unit.[13] This work is currently in progress.

DOI: 10.1021/acs.inorgchem.9b03345
Inorg. Chem. 2020, 59, 1496−1512

■ ASSOCIATED CONTENT

Supporting Information

The Supporting Information is available free of charge at https://pubs.acs.org/doi/10.1021/acs.inorgchem.9b03345.

Supporting Information (1), Physicochemical Data. ^{1}H NMR of H_3tpptac, HRMS spectra of corresponding Eu, Gd, and Tb complexes, pH-dependent UV−visible and pH-dependent ^{1}H NMR data, distribution diagrams for the systems H_3tpptac-La(III), -Gd(III), -Yb(III), -Mn(II), and Ca(II), emission spectra of Eu-tpptac without and in the presence of KF, crystal data and bond angles of the- Tbtpptac complex, and a comparison of the stability constants of H_3tpptac and different chelators with Gd^{3+}, Cu^{2+}, and Zn^{2+} ions (PDF)

Supporting Information (2), Computational Data. Input and output files of the DFT calculations as used with the ADF program are provided, as well as .mol files of the relevant structures. TAPE 21 files are available upon request (ZIP)

Accession Codes

CCDC 1964484 contains the supplementary crystallographic data for this paper. These data can be obtained free of charge via www.ccdc.cam.ac.uk/data_request/cif, or by emailing data_request@ccdc.cam.ac.uk, or by contacting The Cambridge Crystallographic Data Centre, 12 Union Road, Cambridge CB2 1EZ, UK; fax: +44 1223 336033.

■ AUTHOR INFORMATION

Corresponding Authors

*E-mail for L.L.: llamarque@cisbio.com.

*E-mail for C.P.: picard@chimie.ups-tlse.fr.

ORCID

Alberto Lopera: 0000-0001-6482-0081

Estefanía Delgado-Pinar: 0000-0002-7400-5715

René M. Williams: 0000-0002-9490-6182

Jurriaan M. Zwier: 0000-0001-9017-5856

Enrique García-España: 0000-0002-4601-6505

Laurent Lamarque: 0000-0003-1237-7940

Claude Picard: 0000-0002-8770-7732

Author Contributions

The manuscript was written through contributions of all authors. All authors have given approval to the final version of the manuscript.

Notes

The authors declare no competing financial interest.

■ ACKNOWLEDGMENTS

We thank Prof. N. Hildebrandt and Dr. S. Bhuckory (NanoBioPhotonics, Institute for Integrative Biology of the cell (12BC), Université Paris-Saclay, France) for use of equipment and assistance in measuring the high-resolution spectrum. We thank Dr. Stéphane Balayssac for assistance with the recording of the ^{1}H NMR spectrum of the europium complex.

■ REFERENCES

(1) (a) Iman, K.; Shahid, M. Life sensors: current advances in oxygen sensing by lanthanide complexes. *New J. Chem.* **2019**, *43*, 1094−1116. (b) Mathieu, E.; Sipos, A. s.; Demeyere, E.; Phipps, D.; Sakaveli, D.; Borbas, K. E. Lanthanide-based tools for the investigation of cellular environments. *Chem. Commun.* **2018**, *54*, 10021−10035. (c) Zhang, K. Y.; Yu, Q.; Wei, H.; Liu, S.; Zhao, Q.; Huang, W. Long-Lived Emissive Probes for Time-Resolved Photoluminescence Bioimaging and Biosensing. *Chem. Rev.* **2018**, *118*, 1770−1839. (d) Aulsebrook, M. L.; Graham, B.; Grace, M. R.; Tuck, K. L. Lanthanide complexes for luminescence-based sensing of low molecular weight analytes. *Coord. Chem. Rev.* **2018**, *375*, 191−220. (e) Hewitt, S. H.; Butler, S. J. Application of lanthanide luminescence in probing enzyme activity. *Chem. Commun.* **2018**, *54*, 6635−6647. (f) Aletti, A. B.; Gillen, D. M.; Gunnlaugsson, T. Luminescent/colorimetric probes and (chemo-) sensors for detecting anions based on transition and lanthanide ion receptor/binding complexes. *Coord. Chem. Rev.* **2018**, *354*, 98−120. (g) Shuvaev, S.; Starck, M.; Parker, D. Responsive, Water-Soluble Europium(III) Luminescent Probes. *Chem. - Eur. J.* **2017**, *23*, 9974−9989. (h) Zwier, J. M.; Hildebrandt, N. Time-Gated FRET Detection for Multiplexed Biosensing. In *Reviews in Fluorescence 2016*; Geddes, C., Ed.; Springer: 2017; Reviews in Fluorescence. (i) Bünzli, J.-C. G. Lanthanide light for biology and medical diagnosis. *J. Lumin.* **2016**, *170*, 866−878. (j) Sy, M.; Nonat, A.; Hildebrandt, N.; Charbonniere, L. J. Lanthanide-based luminescence biolabelling. *Chem. Commun.* **2016**, *52*, 5080−5095. (k) Zwier, J. M.; Bazin, H.; Lamarque, L.; Mathis, G. Luminescent Lanthanide Cryptates: from the Bench to the Bedside. *Inorg. Chem.* **2014**, *53*, 1854−1866.

(2) Yuan, J.; Wang, G. lanthanide complex-based fluorescence label for time-resolved fluorescence bioassay. *J. Fluoresc.* **2005**, *15*, 559−568.

(3) Thibon, A.; Pierre, V. C. Principles of responsive lanthanide-based luminescent probes for cellular imaging. *Anal. Bioanal. Chem.* **2009**, *394*, 107−120.

(4) Geißler, D.; Hildebrandt, N. Lanthanide Complexes in FRET Applications. *Curr. Inorg. Chem.* **2011**, *1*, 17−35.

(5) Wei, C.; Wei, H.; Yan, W.; Zhao, Z.; Cai, Z.; Sun, B.; Meng, Z.; Liu, Z.; Bian, Z.; Huang, C. Water-Soluble and Highly Luminescent Europium(III) Complexes with Favorable Photostability and Sensitive pH Response Behavior. *Inorg. Chem.* **2016**, *55*, 10645−10653.

(6) Cacheris, W. P.; Nickle, S. K.; Sherry, A. D. Thermodynamic study of lanthanide complexes of 1,4,7-triazacyclononane-N,N',N″-triacetic acid and 1,4,7,10-tetraazacyclododecane-N,N',N″,N‴-tetraacetic acid. *Inorg. Chem.* **1987**, *26*, 958−960.

(7) (a) Leonzio, M.; Melchior, A.; Faura, G.; Tolazzi, M.; Zinna, F.; Di Bari, L.; Piccinelli, F. Strongly Circularly Polarized Emission from Water-Soluble Eu(III)- and Tb(III)-Based Complexes: A Structural and Spectroscopic Study. *Inorg. Chem.* **2017**, *56*, 4413−4421. (b) Laurent, S.; Vander Elst, L.; Galaup, C.; Leygue, N.; Boutry, S.; Picard, C.; Muller, R. N. Bifunctional Gd(III) and Tb(III) chelates based on a pyridine−bis(iminodiacetate) platform, suitable optical probes and contrast agents for magnetic resonance imaging. *Contrast Media Mol. Imaging* **2014**, *9*, 300−312. (c) Takalo, H.; Mukkala, V.-M.; Mikola, H.; Liitti, P.; Hemmila, I. Synthesis of Europium(III) Chelates Suitable for Labeling of Bioactive Molecules. *Bioconjugate Chem.* **1994**, *5*, 278−282.

(8) Nocton, G.; Nonat, A.; Gateau, C.; Mazzanti, M. Water Stability and Luminescence of Lanthanide Complexes of Tripodal Ligands Derived from 1,4,7-Triazacyclononane: Pyridinecarboxamide versus Pyridinecarboxylate Donors. *Helv. Chim. Acta* **2009**, *92*, 2257−2273.

(9) (a) Galland, M.; Le Bahers, T.; Banyasz, A.; Lascoux, N.; Duperray, A.; Grichine, A.; Tripier, R.; Guyot, Y.; Maynadier, M.; Nguyen, C.; Gary-Bobo, M.; Andraud, C.; Monnereau, C.; Maury, O. A ″Multi-Heavy-Atom″ Approach toward Biphotonic Photosensitizers with Improved Singlet-Oxygen Generation Properties. *Chem. - Eur. J.* **2019**, *25*, 9026−9034. (b) Sund, H.; Blomberg, K.; Meltola, N.; Takalo, H. Design of Novel, Water Soluble and Highly Luminescent Europium Labels with Potential to Enhance Immunoassay Sensitivities. *Molecules* **2017**, *22*, 1807. (c) Starck, M.; Pal, R.; Parker, D. Structural Control of Cell Permeability with Highly Emissive Europium(III) Complexes Permits Different Microscopy Applications. *Chem. - Eur. J.* **2016**, *22*, 570−580. (d) Butler, S. J.; Delbianco, M.; Lamarque, L.; McMahon, B. K.; Neil, E. R.; Pal, R.; Parker, D.; Walton, J. W.; Zwier, J. M. EuroTrackerÂ® dyes: design, synthesis,

DOI: 10.1021/acs.inorgchem.9b03345
Inorg. Chem. 2020, 59, 1496−1512

structure and photophysical properties of very bright europium complexes and their use in bioassays and cellular optical imaging. *Dalton Trans.* **2015**, *44*, 4791−4803. (e) Placide, V.; Bui, A. T.; Grichine, A.; Duperray, A.; Pitrat, D.; Andraud, C.; Maury, O. Two-photon multiplexing bio-imaging using a combination of Eu- and Tb-bioprobes. *Dalton Trans.* **2015**, *44*, 4918−4924. (f) Bui, A. T.; Grichine, A.; Brasselet, S.; Duperray, A.; Andraud, C.; Maury, O. Unexpected Efficiency of a Luminescent Samarium(III) Complex for Combined Visible and Near-Infrared Biphotonic Microscopy. *Chem. - Eur. J.* **2015**, *21*, 17757−17761. (g) Delbianco, M.; Sadovnikova, V.; Bourrier, E.; Mathis, G.; Lamarque, L.; Zwier, J. M.; Parker, D. Bright, Highly Water-Soluble Triazacyclononane Europium Complexes To Detect Ligand Binding with Time-Resolved FRET Microscopy. *Angew. Chem., Int. Ed.* **2014**, *53*, 10718−10722. (h) Soulié, M.; Latzko, F.; Bourrier, E.; Placide, V.; Butler, S. J.; Pal, R.; Walton, J. W.; Baldeck, P. L.; Le Guennic, B.; Andraud, C.; Zwier, J. M.; Lamarque, L.; Parker, D.; Maury, O. Comparative Analysis of Conjugated Alkynyl-ChromophoreTriazacyclononane Ligands for Sensitized Emission of Europium and Terbium. *Chem. - Eur. J.* **2014**, *20*, 8636−8646.

(10) Lee, G.; Oka, M.; Takemura, H.; Miyahara, Y.; Shimizu, N.; Inazu, T. Efficient Synthesis of 2,11,20-Triaza[3.3.3](2,6)-pyridinophane. *J. Org. Chem.* **1996**, *61*, 8304−8306.

(11) Castro, G.; Bastida, R.; Macías, A.; Pérez-Lourido, P.; Platas-Iglesias, C.; Valencia, L. Pyridinophane Platform for Stable Lanthanide(III) Complexation. *Inorg. Chem.* **2013**, *52*, 6062−6072.

(12) Castro, G.; Bastida, R.; Macias, A.; Perez-Lourido, P.; Platas-Iglesias, C.; Valencia, L. Lanthanide(III) Complexation with an Amide Derived Pyridinophane. *Inorg. Chem.* **2015**, *54*, 1671−1683.

(13) Leygue, N.; Perez e Iniguez De Heredia, A.; Galaup, C.; Benoist, E.; Lamarque, L.; Picard, C. New advances in the synthesis of tripyridinophane macrocycles suitable to enhance the luminescence of Ln(III) ions in aqueous solution. *Tetrahedron* **2018**, *74*, 4272−4287.

(14) Horrocks, W. D.; Sudnick, D. R. lanthanide ions probes of structure in biology. Laser-induced luminescence decay constants provide a direct measure of the number of metal-coordinated water molecules. *J. Am. Chem. Soc.* **1979**, *101*, 334−340.

(15) Supkowski, R. M.; Horrocks, W. D. W., Jr. On the determination of the number of water molecules, q, coordinated to europium(III) ions in solution from luminescence decay lifetimes. *Inorg. Chim. Acta* **2002**, *340*, 44−48.

(16) Beeby, A.; Clarkson, I. M.; Dickins, R. S.; Faulkner, S.; Parker, D.; Royle, L.; de Sousa, A. S.; Williams, J. A. G.; Woods, M. Non-radiative deactivation of the excited states of europium, terbium and ytterbium complexes by proximate energy-matched OH, NH and CH oscillators: an improved luminescence method for establishing solution hydration states. *J. Chem. Soc., Perkin Trans. 2* **1999**, *2*, 493−504.

(17) Haas, Y.; Stein, G. Pathways of radiative and radiationless transitions in Europium(III) solutions: Role of solvents and anions. *J. Phys. Chem.* **1971**, *75*, 3668−3677.

(18) Ishida, H.; Tobita, S.; Hasegawa, Y.; Katoh, R.; Nozaki, K. Recent advances in instrumentation for absolute emission quantum yield measurements. *Coord. Chem. Rev.* **2010**, *254*, 2449−2458.

(19) Meech, S. R.; Phillips, D. Photophysics of some common fluorescence standarts. *J. Photochem.* **1983**, *23*, 193−217.

(20) (a) Werts, M. H. V.; Jukes, R. T. F.; Verhoeven, J. W. The emission spectrum and the radiative lifetime of Eu^{3+} in luminescent lanthanide complexes. *Phys. Chem. Chem. Phys.* **2002**, *4*, 1542−1548. (b) Beeby, A.; Bushby, L. M.; Maffeo, D.; Williams, J. A. G. Intramolecular sensitisation of lanthanide(III) luminescence by acetophenone-containing ligands: the critical effect of para-substituents and solvent. *J. Chem. Soc., Dalton Trans.* **2002**, 48−54.

(21) Sheldrick, G. A short history of SHELX. *Acta Crystallogr., Sect. A: Found. Crystallogr.* **2008**, *A64*, 112−122.

(22) Sheldrick, G. M. SHELXT - Integrated space-group and crystal-structure determination. *Acta Crystallogr., Sect. A: Found. Adv.* **2015**, *C71*, 3−8.

(23) Garcia-Espana, E.; Ballester, M.-J.; Lloret, F.; Moratal, J. M.; Faus, J.; Bianchi, A. Low-spin six-co-ordinate cobalt(II) complexes. A solution study of tris(violurato)cobaltate(II) ions. *J. Chem. Soc., Dalton Trans.* **1988**, 101−104.

(24) Fontanelli, V.; Micheloni, M. Program for the automatic control of the microburette and the acquisition of the electromotive force readings. *Proceedings of the I Spanish−Italian Congress on Thermodynamic of Metal Complexes*; Peñiscola, Castellón, 1990.

(25) (a) Gran, G. Determination of the equivalence point in potentiometric titrations. Part II. *Analyst* **1952**, *77*, 661−671. (b) Rossotti, J. F.; Rossotti, H. Potentiometric titrations using Gran plots: A textbook omission. *J. Chem. Educ.* **1965**, *42*, 375−378.

(26) Gans, P.; Sabatini, A.; Vacca, A. Investigation of equilibria in solution. Determination of equilibrium constants with the HYPERQUAD suite of programs. *Talanta* **1996**, *43*, 1739−1753.

(27) Alderighi, L.; Gans, P.; Ienco, A.; Peters, D.; Sabatini, A.; Vacca, A. Hyperquad simulation and speciation (HySS): a utility program for the investigation of equilibria involving soluble and partially soluble species. *Coord. Chem. Rev.* **1999**, *184*, 311−318.

(28) Gottlieb, H. E.; Kotlyar, V.; Nudelman, A. NMR Chemical Shifts of Common Laboratory Solvents as Trace Impurities. *J. Org. Chem.* **1997**, *62*, 7512−7515.

(29) Covington, A. K.; Paabo, M.; Robinson, R. A.; Bates, R. G. Use of the Glass Electrode in Deuterium Oxide and the Relation between the Standardized PD (paD) Scale and the Operational pH in Heavy Water. *Anal. Chem.* **1968**, *40*, 700−706.

(30) te Velde, G.; Bickelhaupt, F. M.; Baerends, E. J.; Fonseca Guerra, C.; van Gisbergen, S. J. A.; Snijders, J. G.; Ziegler, T. Chemistry with ADF. *J. Comput. Chem.* **2001**, *22*, 931−967.

(31) Fonseca Guerra, C.; Snijders, J. G.; te Velde, G.; Baerends, E. J. Towards an order-N DFT method. *Theor. Chem. Acc.* **1998**, *99*, 391−403.

(32) van Lenthe, E.; Ehlers, A.; Baerends, E.-J. Geometry optimizations in the zero order regular approximation for relativistic effects. *J. Chem. Phys.* **1999**, *110*, 8943−8953.

(33) Perdew, J. P.; Chevary, J. A.; Vosko, S. H.; Jackson, K. A.; Pederson, M. R.; Singh, D. J.; Fiolhais, C. Atoms, molecules, solids, and surfaces: Applications of the generalized gradient approximation for exchange and correlation. *Phys. Rev. B: Condens. Matter Mater. Phys.* **1992**, *46*, 6671−6687.

(34) (a) Christoffers, J.; Starynowicz, P. A europium(II) complex with bis-pyridino-18-crown-6. *Polyhedron* **2008**, *27*, 2688−2692. (b) Vidjayacoumar, B.; Ilango, S.; Ray, M. J.; Chu, T.; Kolpin, K. B.; Andreychuk, N. R.; Cruz, C. A.; Emslie, D. J. H.; Jenkins, H. A.; Britten, J. F. Rigid NON- and NSN-ligand complexes of tetravalent and trivalent uranium: comparison of U-OAr_2 and U-SAr_2 bonding. *Dalton Trans.* **2012**, *41*, 8175−8189.

(35) Pettersen, E. F.; Goddard, T. D.; Huang, C. C.; Couch, G. S.; Greenblatt, D. M.; Meng, E. C.; Ferrin, T. E. UCSF Chimera - A visualization system for exploratory research and analysis. *J. Comput. Chem.* **2004**, *25*, 1605−1612.

(36) Tircso, G.; Kovacs, Z.; Sherry, A. D. Equilibrium and Formation/Dissociation Kinetics of Some Ln^{III}PCTA Complexes. *Inorg. Chem.* **2006**, *45*, 9269−9280.

(37) Valencia, L.; Martinez, J.; Macias, A.; Bastida, R.; Carvalho, R. A.; Geraldes, C. F. G. C. X-ray Diffraction and ^{1}H NMR in Solution: Structural Determination of Lanthanide Complexes of a $Py_2N_6Ac_4$ Ligand. *Inorg. Chem.* **2002**, *41*, 5300−5312.

(38) Chen, D.; Squattrito, P. J.; Martell, A. E.; Clearfield, A. Synthesis and Crystal Structure of a Nine-Coordinate Gadolinium-(III) Complex of 1,7,13-Triaza-4,10, 16-trioxacyclooctadecane-N,N′,N″-triacetic acid. *Inorg. Chem.* **1990**, *29*, 4366−4368.

(39) (a) Alexander, V. Design and Synthesis of Macrocyclic Ligands and Their Complexes of Lanthanides and Actinides. *Chem. Rev.* **1995**, *95*, 273−342. (b) Gueye, N. M.; Moussa, D.; Thiam, E. I.; Barry, A. H.; Gaye, M.; Retailleau, P. Crystal structure of bis(acetato-κ^2O,O')diaqua[1-(pyridin-2-ylmethylidene-κN)-2-(pyridin-2-yl-κN)-hydrazineκN^1]terbium(III) nitrate monohydrate. *Acta Cryst. E* **2017**, *73*, 1121−1124.

DOI: 10.1021/acs.inorgchem.9b03345
Inorg. Chem. 2020, 59, 1496−1512

(40) Siaugue, J.-M.; Favre-Réguillon, A.; Dioury, F.; Plancque, G.; Foos, J.; Madic, C.; Moulin, C.; Guy, A. Effect of Mixed Pendant Groups on the Solution Properties of 12-Membered Azapyridinomacrocycles: Evaluation of the Protonation Constants and the Stability Constants of the Europium(III) Complexes. *Eur. J. Inorg. Chem.* **2003**, *2003*, 2834−2838.
(41) Stetter, H.; Frank, W.; Mertens, R. Darstellung und komplexbildung von polyazacycloalkan-N-essigsäuren. *Tetrahedron* **1981**, *37*, 767−772.
(42) Kim, W. D.; Hrncir, D. C.; Kiefer, G. E.; Sherry, A. D. Synthesis, Crystal Structure, and Potentiometry of Pyridine-Containing Tetraaza Macrocyclic Ligands with Acetate Pendant Arms. *Inorg. Chem.* **1995**, *34*, 2225−2232.
(43) Miao, L.; Bell, D.; Rothremel, G. L.; Bryant, L. H.; Fitzsimmons, P. M.; Jackels, S. C. Design and synthesis of an ″ultrachelating″ ligand based on an 18-membered ring hexaaza macrocycle. *Supramol. Chem.* **1996**, *6*, 365−373.
(44) Delgado, R.; Sun, Y.; Motekaitis, R. J.; Martell, A. E. Stabilities of divalent and trivalent metal ion complexes of macrocyclic triazatriacetic acids. *Inorg. Chem.* **1993**, *32*, 3320−3326.
(45) Takacs, A.; Napolitano, R.; Purgel, M.; Csaba Benyei, A.; Zekany, L.; Brücher, E.; Toth, I.; Baranyai, Z.; Aime, S. Solution Structures, Stabilities, Kinetics, and Dynamics of DO3A and DO3A-Sulphonamide Complexes. *Inorg. Chem.* **2014**, *53*, 2858−2872.
(46) (a) Bonnet, C. S.; Buron, F.; Caillé, F.; Shade, C. M.; Drahos, B.; Pellegatti, L.; Zhang, J.; Villette, S.; Helm, L.; Pichon, C.; Suzenet, F.; Petoud, S.; Toth, E. Pyridine-based lanthanide complexes combining MRI and NIR luminescence activities. *Chem. - Eur. J.* **2012**, *18*, 1419−1431. (b) Chatterton, N.; Gateau, C.; Mazzanti, M.; Pécaut, J.; Borel, A.; Helm, L.; Merbach, A. The effect of pyridinecarboxylate chelating groups on the stability and electronic relaxation of gadolinium complexes. *Dalton Trans.* **2005**, 1129−1135.
(47) Kodama, M.; Koike, T.; Mahatma, A. B.; Kimura, E. Thermodynamic and kinetic studies of lanthanide complexes of 1,4,7,10,13-pentaazacyclopentadecane-N,N',N",N"',N""-pentaacetic acid and 1,4,7,10,13,16-hexaazacyclooctadecane-N,N',N",N"',N"",N""'-hexaacetic acid. *Inorg. Chem.* **1991**, *30*, 1270−1273.
(48) Roca-Sabio, A.; Bonnet, C. S.; Mato-Iglesias, M.; Esteban-Gomez, D.; Toth, E.; Blas, A.; Rodriguez-Blas, T.; Platas-Iglesias, C. Lanthanide Complexes Based on a Diazapyridinophane Platform Containing Picolinate Pendants. *Inorg. Chem.* **2012**, *51*, 10893−10903.
(49) Gündüz, S.; Vibhute, S.; Botar, R.; Kalman, F. K.; Toth, I.; Tircso, G.; Regueiro-Figueroa, M.; Esteban-Gomez, D.; Platas-Iglesias, C.; Angelovski, G. Coordination Properties of GdDO3A-Based Model Compounds of Bioresponsive MRI Contrast Agents. *Inorg. Chem.* **2018**, *57*, 5973−5986.
(50) Bianchi, A.; Calabi, L.; Corana, F.; Fontana, S.; Losi, P.; Maiocchi, A.; Paleari, L.; Valtancoli, B. Thermodynamic and structural properties of Gd(III) complexes with polyamino-polycarboxylic ligands: basic compounds for the development of MRI contrast agents. *Coord. Chem. Rev.* **2000**, *204*, 309−393.
(51) (a) Houlne, M. P.; Agent, T. S.; Kiefer, G. E.; McMillan, K.; Bornhop, D. J. Spectroscopic Characterization and Tissue Imaging Using Site-Selective Polyazacyclic Terbium(III) Chelates. *Appl. Spectrosc.* **1996**, *50*, 1221−1228. (b) Siaugue, J.-M.; Segat-Dioury, F.; Favre-Reguillon, A.; Wintgens, V.; Madic, C.; Foos, J.; Guy, A. Europium(III) complex formed with pyridine containing azamacrocyclic triacetate ligand: characterization by sensitized Eu(III) luminescence. *J. Photochem. Photobiol., A* **2003**, *156*, 23−29. (c) Bechara, G.; Leygue, N.; Galaup, C.; Mestre-Voegtlé, B.; Picard, C. Polyazamacrocycles based on a tetraaminoacetate moiety and a (poly)pyridine intracyclic unit: direct synthesis and application to the photosensitization of Eu(III) and Tb(III) ions in aqueous solutions. *Tetrahedron* **2010**, *66*, 8594−8604.
(52) Enel, M.; Leygue, N.; Saffon, N.; Galaup, C.; Picard, C. Facile Access to the 12-Membered Macrocyclic Ligand PCTA and Its Derivatives with Carboxylate, Amide, and Phosphinate Ligating Functionalities. *Eur. J. Org. Chem.* **2018**, *2018*, 1765−1773.
(53) Le Fur, M.; Molanr, E.; Beyler, M.; Fougère, O.; Esteban-Gomez, D.; Rousseaux, O.; Tripier, R.; Tircso, G.; Platas-Iglesias, C. Expanding the Family of Pyclen-Based Ligands Bearing Pendant Picolinate Arms for Lanthanide Complexation. *Inorg. Chem.* **2018**, *57*, 6932−6945.
(54) Mathis, G.; Dumont, C.; Jolu, E.J.-P. Method using fluoride ion for reducing interference in a fluorescence assay. Patent WO 92:01224, 1992.
(55) (a) Zhuravlev, K. P.; Tsaryuk, V. I.; Vologzhanina, A. V.; Gawryszewska, P. P.; Kudryashova, V. A.; Klemenkova, Z. S. Crystal Structures of New Lanthanide Hydroxybenzoates and Different Roles of LMCT State in the Excitation Energy Transfer to Eu3+ Ions. *ChemistrySelect* **2016**, *1*, 3428−3437. (b) Sabbatini, N.; Guardigli, M.; Lehn, J.-M. Luminescent lanthanide complexes as photochemical supramolecular devices. *Coord. Chem. Rev.* **1993**, *123*, 201−228.
(56) Binnemans, K. Interpretation of europium(III) spectra. *Coord. Chem. Rev.* **2015**, *295*, 1−45.
(57) (a) Janicki, R.; Mondry, A. Thermodynamics of the hydration equilibrium derived from the luminescence spectra of the solid state for the case of the Eu-EDTA system. *Phys. Chem. Chem. Phys.* **2015**, *17*, 29558−29565. (b) Mato-Iglesias, M.; Roca-Sabio, A.; Palinkas, Z.; Esteban-Gomez, D.; Platas-Iglesias, C.; Toth, E.; de Blas, A.; Rodriguez-Blas, T. Lanthanide Complexes Based on a 1,7-Diaza-12-crown-4 Platform Containing Picolinate Pendants: A New Structural Entry for the Design of Magnetic Resonance Imaging Contrast Agents. *Inorg. Chem.* **2008**, *47*, 7840−7851. (c) Platas-Iglesias, C.; Corsi, D. M.; Elst, L. V.; Muller, R. N.; Imbert, D.; Bünzli, J.-C. G.; Toth, E.; Maschmeyer, T.; Peters, J. A. Stability, structure and dynamics of cationic lanthanide(iii) complexes of N,N'-bis-(propylamide)ethylenediamine-N,N'-diacetic acid. *Dalton Trans.* **2003**, 727−737.
(58) Frey, S. T.; Horrocks, W. D. On correlating the frequency of the $^7F_0 \rightarrow {}^5D_0$ transition in Eu^{3+} complexes with the sum of 'nephelauxetic parameters' for all of the coordinating atoms. *Inorg. Chim. Acta* **1995**, *229*, 383−390.
(59) (a) Latva, M.; Takalo, H.; Mukkala, V.-M.; Kankare, J. Evaluation of solution structures of highly luminescent europium(III) chelates by using laser induced excitation of the $^7F_0 \rightarrow {}^5D_0$ transition. *Inorg. Chim. Acta* **1998**, *267*, 63−72. (b) Latva, M.; Kankare, J. THE $^7F_0 \rightarrow {}^5D_0$ EXCITATION SPECTRA OF EUROPIUM(III) COMPLEXES OF AMINOCARBOXYLIC ACIDS. *J. Coord. Chem.* **1998**, *43*, 121−142.
(60) Bünzli, J.-C. G.; Piguet, C. Taking advantages of luminescent lanthanide ions. *Chem. Soc. Rev.* **2005**, *34*, 1048−1077.
(61) (a) Kim, W. D.; Kiefer, G. E.; Maton, F.; McMillan, K.; Muller, R. N.; Sherry, A. D. Relaxometry, Luminescence Measurements, Electrophoresis, and Animal Biodistribution ofLanthanide(III) Complexes of Some Polyaza Macrocyclic Acetates Containing Pyridine. *Inorg. Chem.* **1995**, *34*, 2233−2243. (b) Takalo, H.; Hanninen, E.; Kankare, J. The influence of substituents on the luminescence properties of the Eu(III) and Tb(III) chelates of 4-(phenylethynyl)pyridine derivatives. *J. Alloys Compd.* **1995**, *225*, 511−514.
(62) (a) Latva, M.; Takalo, H.; Mukkala, V.-M.; Matachescu, C.; Rodriguez-Ubis, J.-C.; Kankare, J. Correlation between the lowest triplet state energy level of the ligand and lanthanide(III) luminescence quantum yield. *J. Lumin.* **1997**, *75* (b), 149−169.
(63) (a) Xiao, M.; Selvin, P. R. Quantum Yields of Luminescent Lanthanide Chelates and Far-Red Dyes Measured by Resonance Energy Transfer. *J. Am. Chem. Soc.* **2001**, *123*, 7067−7073. (b) Li, M.; Selvin, P. R. Luminescent polyaminoacicarboxylate chelates of terbium and europium: the effect of chelate structure. *J. Am. Chem. Soc.* **1995**, *117*, 8132−8138.
(64) Guillou, A.; Lima, L. M. P.; Roger, M.; Esteban-Gomez, D.; Delgado, R.; Platas-Iglesias, C.; Patinec, V.; Tripier, R. 1,4,7-Triazacyclononane-Based Bifunctional Picolinate Ligands for Efficient Copper Complexation. *Eur. J. Inorg. Chem.* **2017**, *2017*, 2435−2443.

DOI: 10.1021/acs.inorgchem.9b03345
Inorg. Chem. 2020, 59, 1496−1512

(65) Aime, S.; Batsanov, A. S.; Botta, M.; Dickins, R. S.; Faulkner, S.; Foster, C. E.; Harrison, A.; Howard, J. A. K.; Moloney, J. M.; Norman, T. J.; Parker, D.; Royle, L.; Williams, J. A. G. Nuclear magnetic resonance, luminescence and structural studies of lanthanide complexes with octadentate macrocyclic ligands bearing benzylphosphinate groups. *J. Chem. Soc., Dalton Trans.* **1997**, 3623−3636.

DOI: 10.1021/acs.inorgchem.9b03345
Inorg. Chem. 2020, 59, 1496−1512